Atmospheric Pollution Research 17 (2026) 102965

Contents lists available at ScienceDirect

Atmospheric Pollution Research

journal homepage: www.elsevier.com/locate/apr

The impact of synoptic forcing and vehicle traffic on atmospheric transport processes and NO_2 concentrations in a highly polluted urban street canyon

Leyla Sungur [a,e,*], Ines Bamberger [b], Johann Schneider [a], Frederik Bachmann [c], Anke C. Nölscher [b,d], Christoph K. Thomas [a,d]

[a] University of Bayreuth, Micrometeorology Group, Bayreuth, Germany
[b] University of Bayreuth, Atmospheric Chemistry, Bayreuth, Germany
[c] Technical University of Munich, Munich, Germany
[d] University of Bayreuth, BayCEER, Bayreuth Center of Ecology and Environmental Research, Bayreuth, Germany
[e] Climate Service Center Germany (GERICS), Helmholtz Zentrum Hereon, Hamburg, Germany

ARTICLE INFO

Keywords:
Nitrogen dioxide
Urban air pollution
Vehicle-induced turbulence
Atmospheric transport

ABSTRACT

Ongoing air quality issues persist in Munich, Germany's third most populous city, where annual nitrogen dioxide (NO_2) concentrations have exceeded national standards at a key monitoring station prior to 2024 since measurements began. According to European legislation, air quality plans must be implemented to address such exceedance. Additionally, upcoming revisions to EU regulations aim to halve the current annual threshold of 40 μg m^{-3} making effective reduction strategies essential. This study investigates the role of atmospheric transport processes in contributing to NO_2 concentration exceedances within a densely built urban street canyon characterized by heavy traffic and poor ventilation. Using a two-year observational campaign (2021–2023) alongside high-resolution Large Eddy Simulations (LES) with the PALM-4U model, we analyze the effects of wind direction, speed, turbulent kinetic energy (TKE), and traffic dynamics on pollutant concentrations. Ultrasonic anemometers and simulation scenarios focus on the two most relevant local flow regimes: a common northerly flow (44%) and a less frequent westerly flow in the urban canyon. Findings show that the dominant northerly flow is decoupled of large-scale synoptic conditions and leads to pollutant accumulation and daily averaged NO_2 concentration reaching up to 72 μg m^{-3}. Vehicle-induced turbulence has a non-linear relationship with NO_2 concentrations, highlighting the strong influence of diurnal traffic patterns. These results underscore that both emission reduction and enhanced air mixing are vital to mitigating urban air pollution in this street canyon. Addressing this dual challenge is crucial to meeting future air quality targets and safeguarding public health in urban environments.

1. Introduction

NO_2 is a critical atmospheric pollutant with adverse implications for human health and vegetation at elevated concentrations (Phoenix et al., 2012; Costa et al., 2014). This pollutant enters the atmosphere through two primary mechanisms: direct emissions, mainly from anthropogenic sources such as fossil fuel combustion for energy production, heating, and transportation, and secondary formation through photochemical reactions (Wang et al., 2025). These secondary processes include the interaction of ozone (O_3) with nitric oxide (NO) and the oxidation of hydrocarbons in the presence of NO (Fino, 2019; Wang et al., 2025). In urban settings, both pathways contribute significantly to the concentration of ambient NO_2, their relative importance being influenced by proximity to emission sources and temporal factors, such as diurnal and seasonal variability (Anttila et al., 2011; Kurtenbach et al., 2012).

The impact of urban air quality on public health is especially critical in densely populated areas, where motor vehicle emissions introduce pollutants directly into the ambient environment. Along high-traffic corridors, spatial confinement of nitrogen dioxides

$$NO_x = NO + NO_2 \quad (1)$$

and reduced atmospheric mixing due to urban infrastructure often result in the exceedance of regulatory thresholds. NO_2 is an irritant gas (von Nieding et al., 1970). Higher concentrations contribute to respiratory tract irritation through mucosal absorption, which can affect pulmonary function and weaken immune responses (von Nieding et al., 1970). Prolonged exposure to elevated NO_2 is correlated with an increased incidence of respiratory infections and an increased risk of cardiovascular disease (Anenberg et al., 2022; Huang et al., 2021).

* Correspondence to: Universität Bayreuth, Universitätsstraße 30, 95444 Bayreuth.
E-mail address: leyla.sungur@uni-bayreuth.de (L. Sungur).

https://doi.org/10.1016/j.apr.2026.102965
Received 4 July 2025; Received in revised form 16 February 2026; Accepted 18 February 2026
Available online 19 February 2026

Efforts to regulate NO_2 concentrations have led to the establishment of air quality standards, although the determination of safe exposure limits remains a subject of ongoing scientific investigation. Studies advocate for more stringent limits (Di et al., 2017). In Germany, the 39th Ordinance to the BImSchG (39. BImSchV) sets the national standard for ambient air quality, aligning with European Union directives, setting the annual mean national air quality standard for NO_2 at 40 micrograms per cubic meter μg $m^{-}3$. The hourly mean should not exceed 200 μg $m^{-}3$ more than 18 times per calendar year. These thresholds are designed to protect human health and are enforced through continuous monitoring and reporting by environmental agencies. Emissions of nitrogen oxides from road transport have not decreased sufficiently, and NO_2 ambient concentration, especially at roadside sites, has not decreased as expected (Casquero-Vera et al., 2019). Several studies have show European cities still exceeding the annual NO_2 air quality limit value and that NO_2 exceedances are connected to road traffic (Guerreiro et al., 2014; Font and Fuller, 2016; Casquero-Vera et al., 2019; Kurtenbach et al., 2012). Exceedings lead to the implementation of air quality plans and measures aimed at reducing NO_2 emissions, particularly in urban areas with high traffic density.

The atmospheric concentration of NO_2 in urban environments is modulated by various physical processes, including transport, ventilation, dilution, and turbulent mixing within the urban boundary layer (Guerreiro et al., 2014). In addition to variations in NO_2 emission strengths, atmospheric concentrations are influenced by degradation processes such as photolysis under solar radiation, chemical reactions with hydrocarbons, and deposition in vegetation, all of which are spatially and temporally variable (Kuhlmann et al., 2022). NO_2 undergoes rapid photolysis in the presence of sunlight. Upon reaction with oxygen, it produces NO and O_3, contributing to near-ground O_3 formation and establishing NO_2 as a primary O_3 precursor (Kurtenbach et al., 2012; Pandey and Singh, 2021). Beyond its role in O_3 formation, NO_2 is involved in the formation of particulate matter, both being secondary pollutants themselves (Yang et al., 2018). Thus, the dynamic interaction between the sources and sinks of NO_2, combined with their reactivity, makes NO_2 a key precursor in atmospheric chemistry, contributing to both photochemical smog and air quality degradation (Sun et al., 2024; Wang et al., 2025). Current regional and city-scale changes in atmospheric NO_2 are consistently monitored through ongoing research in Europe (see Amritha et al. (2024), Guerreiro et al. (2014), Kurtenbach et al. (2012)). Casquero-Vera et al. and Kurtenbach et al. investigated the impact of primary NO_2 emissions at various urban sites that exceed the standard limit of the European NO_2. Stewart et al. work on air pollution forecast in Europe for NO_x and NO_2 vehicle emission curves. Current studies investigate how to reduce NO_2 concentrations more efficiently (Anttila et al., 2011; Casquero-Vera et al., 2019). Several studies have examined the impact of traffic-related NO_2 reduction strategies, highlighting challenges in achieving substantial improvements (El-Hansali et al., 2021; Baldasano et al., 2010; Kurtenbach et al., 2012). Research on the role of urban structure has emerged (see Pültz et al. (2025)) and also the impact of atmospheric processes has been considered in studies using a multimodal intermediate fusion with satellite imagery (Zhang et al. (2025)) or model environment (Dai et al. (2022)). However, there remains a critical gap in understanding the role of atmospheric transport processes on a local scale, particularly within dense urban street canyons where geometry, turbulence, and thermodynamic conditions interact in complex ways. The dynamics of air pollution are intrinsically linked to meteorological conditions, as atmospheric flows are governed by the principles of fluid mechanics described by the Navier–Stokes equations. Advances in computational capabilities have substantially accelerated progress in air quality modeling, facilitating increasingly detailed and accurate simulations. Recent developments in high-resolution modeling, especially Large Eddy Simulation (LES), have made it possible to resolve turbulent flow structures and pollutant transport at the urban scale with greater fidelity (Maronga et al., 2019; Zhiyin, 2015). LES is uniquely capable of capturing the three-dimensional time-dependent dynamics of urban atmospheric processes, providing valuable information on localized pollution patterns. While validation is a crucial step in the application of numerical models, it is still rarely carried out in a fully quantitative manner using observational data, primarily due to the limited availability of sufficiently comparable variables. For flow fields around buildings, wind-tunnel experiments have therefore often been used as reference data, benefiting from their highly controlled conditions (Okaze et al., 2021). Similar approaches have been widely applied for the validation of passive pollutant concentration fields and atmospheric boundary-layer dispersion (Bazdidi-Tehrani et al., 2020; Kellneróva et al., 2018; Moonen et al., 2013). For the evaluation of operational dispersion air quality models, LES comparison has been performed (Grylls et al., 2019) using the model uDALES. An evaluation of the PALM 6.0 LES model by Maronga et al. (2020) served as a pilot study for explicit PALM LES validation and compared model results of surface temperature, air temperature, wind speed as well as wall heat flux and concentrations of NO_x and PM10 with measurement campaigns as time series comparisons. In an explicit PALM validation pilot study with a large observational network featuring air temperature, wind speed, wind direction and humidity, Sungur et al. have shown the ability of space–time variability of scalars and wind fields using PALM 23.10. Sungur et al. (2025). In accordance with evolving European Union regulations, Large Eddy Simulation (LES) techniques provide a robust framework for spatially resolving NO_2 distributions in urban environments, offering critical insights to inform policy decisions and public health interventions. Despite these advances, few studies integrate in situ turbulence measurements with LES modeling to analyze pollution transport in weakly ventilated street canyons - particularly those oriented perpendicular to the prevailing synoptic flow, where mixing is further suppressed.

This study aims to bridge this gap by applying a holistic approach that combines ultrasonic anemometry and flow-resolving LES modeling. Focusing on a highly polluted, traffic-dense urban canyon, we investigate the impact of atmospheric transport, traffic-induced turbulence, and synoptic forcing on NO_2 dispersion. Our case study represents a typical worst-case scenario: a street canyon with high emissions and minimal natural ventilation, serving as a testbed to assess the spatial dynamics of pollutant transport under contemporary European regulatory and urban planning conditions. Our study serves as a case study for an extremely weak-mixing location with very high traffic density, the street canyon orientation being perpendicular to the regional main synoptic flow regime. The presented study area is a high traffic street canyon located amidst the city of Munich, Germany. A long-term monitoring station operated by the state of Bavaria records airborne NO_2 concentrations (Bayerisches Staatsministerium für Umwelt und Verbraucherschutz, 2025). Despite a consistent downward trend, NO_2 annual averages remained elevated, measuring 54 μg $m^{-}3$ in 2020, 51 μg $m^{-}3$ in 2021, 49 μg $m^{-}3$ in 2022, and 45 μg $m^{-}3$ in 2023. During our study period in 2024, the annual mean concentration decreased to 39 μg $m^{-}3$, marking the first time it fell below national air quality standards.

In our study, we pose the following research questions:

(A) What is the prevailing flow regime within the studied street canyon (Aspect Ratio 0.37), and does it exhibit wake interference flow characteristics?
(B) How does the interaction between synoptic forcing and thermal effects influence local wind fields and turbulent mixing?
(C) How do atmospheric transport dynamics contribute to the diurnal variability of NO_2 concentrations within the canyon?

To address these questions, our study pursues the following objectives:

1. Classify the local flow regime of the canyon in the context of its low aspect ratio (0.37) and high vehicle load, evaluating whether the conditions align with wake interference flow and synoptic wind direction.

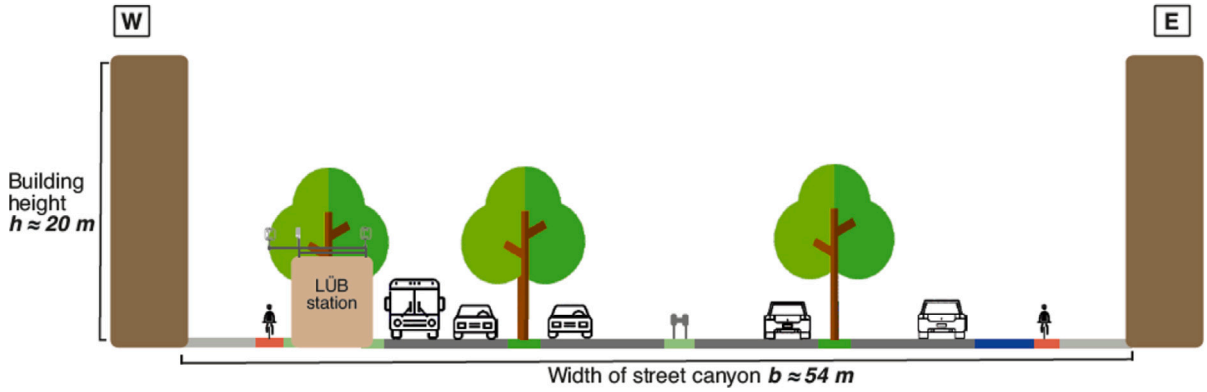

Fig. 1. Schematic study site consisting of an 8 lane street canyon of approx. 50 m width and buildings of 20 m height. The road is planted on the sides and between the outer and inner lanes.

2. To evaluate the diurnal evolution of NO_2 concentrations in relation to traffic patterns, solar-induced thermal effects, and atmospheric transport processes.
3. Quantify the spatial and temporal variation of the turbulent mixing and vehicle-induced turbulence within the canyon.

This integrated approach provides a detailed understanding of local-scale transport processes in complex urban environments and supports improved modeling of pollutant behavior in street canyon settings.

2. Methods and material

2.1. Study area

The city of Munich is Germany's third largest city with a registered population of 1.5 million people. The location in which we conduct our study is an 8-lane road oriented in a north–south direction through the Neuhausen-Nymphenburg district of Munich, forming part of the city's central ring road of 4.5 km length. The street canyon has a width of 54 m and is surrounded by buildings of approximately 20 m height on the west and east sides, as illustrated in Fig. 1, 2 3. Vegetation occurs along the sides of the road and between the outer and inner lanes. The canyon of the street covers the main traffic of vehicles with a destination outside the city. The Aspect Ratio is approx. 0.37. The vehicle fleet consists of passenger cars, trucks, and delivery vans with an additional bus line introduced in 2023.

A tunnel located in the northern part of the study area is expected to significantly influence local NO_2 concentration levels. As the tunnel lacks an internal filtration system, there is no mechanism to reduce NO_2 emissions within it. Given the relatively small internal volume of the tunnel, pollutants tend to accumulate and are transported from north to south by vehicle-induced airflow. This process is expected to lead to elevated concentrations of NO_2 at the southern exit of the tunnel, particularly on the western side of the road.

2.2. Observational study

The air quality monitoring station (AQS) has been operated by the state environmental authority (LfU) since 2004 and is located on the western side of the road, between the approach to a bridge in the south and a tunnel exit in the north. This station is classified as an urban location close to traffic and measures air pollutants and meteorological parameters, including carbon monoxide, nitrogen oxides (NO, NO_2), particulate matter (PM2.5 and PM10), constituents of PM10, hydrocarbons (benzene, toluene, and xylene), dust precipitation, air temperature, and relative humidity. Identical to the location of the air quality station, our study was conducted on the western side of the street canyon. The turbulent and advective transport of air was characterized using high-resolution three-dimensional ultrasonic anemometers, (specifically the uSonic-3 Multi-Path model (METEK GmbH, 2023)). Such instruments determine air movement (velocity and direction) along the measurement path by measuring the transit time of acoustic pulses between paired transceivers (Foken, 2021). Two turbulence measurement systems were developed, each incorporating an ultrasonic anemometer and a micro-weather station (METER Group, Inc., 2021) (see Fig. 2). By combining signals from three non-orthogonal measurement paths, the three-dimensional instantaneous turbulent wind components u, v, and w were derived. One further measurement complex was equipped with high resolution pressure wave sensors to capture traffic volume. The functionality of all stations was validated under controlled laboratory conditions prior to field deployment. The measurements were performed with a sampling frequency of 20 Hz.

The systems were mounted on the roof of the air quality station to independently estimate traffic volumes and assess their impact on local turbulence patterns (see Fig. 2). One sonic anemometer was installed facing the sidewalk and the bicycle path (see Fig. 2b) black circle), while the second was positioned towards the roadway to capture and analyze turbulence generated by vehicular traffic (see Fig. 2b) red circle) with an absolute distance of 4.50 m. The second turbulence measurement complex was kept at the site of the AQS for the whole experimental period between 06/2021 - 10/2022. To facilitate a direct comparison of flow strength and direction, the sidewalk turbulence measurement complex was further operated at alternating locations on the western side of the investigated street canyon (see M1 - M3 in Fig. 2). This semi-stationary deployment spanned two to three months each and aimed to capture the spatial variability of turbulent and advective flow within the study area. Table 1 shows all measurements which were taken for this study.

To investigate the spatial distribution of NO_2 within the street canyon and its adjacent areas, we performed high-resolution measurements using a mobile air quality monitoring system. Atmospheric NO_2 concentrations were measured using a mobile cavity attenuated phase shift (CAPS) spectroscopy-based device (Teledyne T500U), selected for its high precision and direct detection capabilities without interference, as described by Kebabian et al. (2008) and Ge et al. (2013). The technique employs a modulated square wave signal at 440 nm, which NO_2 characteristically shifts, allowing unambiguous quantification. To compare the mobile CAPS with the standardized measurements of the AQS, both instruments were operated side by side at the AQS for a period of three weeks (2021-06-16 - 2021-07-14). A direct comparison between the stationary chemiluminescence device at the air quality station and the mobile CAPS demonstrated good agreement within 14%, with an offset of 6 $\mu g\ m^{-3}$. Hence, the mobile CAPS was deployed at three different locations from 2021/12–2022/06, 2022/06–2022/10, 2022/11–2023/08 on the western side of the investigated street canyon (see Fig. 2). Measurements were carried out with air sampling performed at a lower measurement height of 1.9 m above ground-level.

Fig. 2. (a) Closeup of the spatial distribution of the study area and its locations of measurements. The schematic pictures the exact area and land cover of the LES child domain of the study site consisting of an 8 lane street canyon of approx. 50 m width and buildings of 20 m height. M1 - M3 represent the alternating meteorological mobile measurement locations, CAPS 1–3 represent the alternating chemical measurement locations. (b) measurement devices of ultrasonic anemometer for roadside (red), windspeed, wind direction and temperature (purple), ultrasonic anemometer for pedestrian lane (black), mean NO_2 concentration (yellow).

Table 1
Tabular of meteorological and air quality variables measured in the study area.

Variable	Observation period	Observation time interval	Location	Unit
Turbulent u	16-Jul-2021 until 20-Jun-2023	50 ms (20 Hz)	AQS (street)	m/s
Turbulent v	16-Jul-2021 until 20-Jun-2023	50 ms (20 Hz)	AQS (street)	m/s
Turbulent w	16-Jul-2021 until 20-Jun-2023	50 ms (20 Hz)	AQS (street)	m/s
Turbulent sonic temperature	16-Jul-2021 until 20-Jun-2023	50 ms (20 Hz)	AQS (street)	K
Turbulent barometric pressure	16-Jul-2021 until 20-Jun-2023	50 ms (20 Hz)	AQS (street)	hpa
Turbulent u	08-Jun-2021 until 24-Jun-2022	50 ms (20 Hz)	AQS (bikelane)	m/s
Turbulent v	08-Jun-2021 until 24-Jun-2022	50 ms (20 Hz)	AQS (bikelane)	m/s
Turbulent w	08-Jun-2021 until 24-Jun-2022	50 ms (20 Hz)	AQS (bikelane)	m/s
Turbulent sonic temperature	08-Jun-2021 until 24-Jun-2022	50 ms (20 Hz)	AQS (bikelane)	K
air temperature	16-Jul-2021 until 20-Jun-2023	10 min	AQS	K
air pressure	16-Jul-2021 until 20-Jun-2023	10 min	AQS	hpa
relative humidity	16-Jul-2021 until 20-Jun-2023	10 min	AQS	%
incoming solar radiation	16-Jul-2021 until 20-Jun-2023	10 min	AQS	W m/s
wind speed	16-Jul-2021 until 20-Jun-2023	10 min	AQS	m/s
wind direction	16-Jul-2021 until 20-Jun-2023	10 min	AQS	degree
precipitation	16-Jul-2021 until 20-Jun-2023	10 min	AQS	mm
NO_2, PM10 (LfU)	01-Jan-2021 until 31-Jul-2023	60 min	AQS	ppb
NO_2 (UBT)	15-Dec-2021 until 01-Jun-2023	30 min	Landshuter Allee	ppb

The system, complemented by a UV absorption ozone analyzer, continuously provided NO_2 data with a temporal resolution of 1 min from 2021-12 to 2022-06. These measurements aimed to improve our understanding of the air quality drivers along the investigated street canyon.

To better understand the influence of turbulent mixing and advection on ground level NO_2 concentrations in a high-traffic street canyon flanked by tall buildings, a long-term analysis of synoptic forcing conditions and allocation to the corresponding large-scale weather conditions was performed using data recovered from the air quality station and the city meteorological reference station. Based on the availability of a complete and coherent data set over a long time period, meteorological data from 2015 to 2016 was analyzed. The airflow regimes were computed and compared at the city's meteorological reference station and the local air quality station in the street canyon. The statistical

turbulent metrics relevant to mixing and transport in this study were calculated using the temporal deviations of various variables measured. To compute atmospheric turbulent fluxes of momentum, sensible heat, and other metrics, Reynolds decomposition

$$x = \overline{x} + x', \tag{2}$$

are used. The instantaneous measurement data was applied, allowing for the separation of mean transport from turbulent transport. A perturbation time scale of 30 min was chosen on the basis of turbulence spectra. Other key turbulent metrics include

1. The vertical wind variance (or its square root):

$$\sigma_w = \sqrt{\overline{w'w'}}, \tag{3}$$

2. The vertical turbulence intensity:

$$TI_w = \frac{\sigma_w}{\overline{U}}, \tag{4}$$

3. The turbulent kinetic energy:

$$TKE = \frac{1}{2}\left(\overline{u'u'} + \overline{v'v'} + \overline{w'w'}\right), \tag{5}$$

4. The density-normalized momentum flux, represented as shear stress velocity:

$$u_* = \sqrt{\overline{u'w'}^2 + \overline{v'w'}^2}, \tag{6}$$

5. The kinematic heat flux:

$$q_h = \overline{w'\theta'}. \tag{7}$$

The first three metrics quantify turbulent mixing in the air, while the latter two characterize the transfer of momentum between the air flow and the surface, as well as the heating or cooling of the air. Furthermore, mean climatic variables such as air temperature, humidity, solar radiation, precipitation, air pressure, and wind direction and speed were recorded using micro-weather stations with a time-averaging interval of 5 min.

2.3. LES model simulation

Our modeling approach consists of high-resolution, turbulence-resolving atmospheric simulations to identify and explain characteristic flow regimes and gain process-oriented insights derived from empirical data. The PALM-4U LES model was adapted and extended using the urban modeling packages provided within the PALM-4U framework. The core study area of the street canyon was modeled with an isotropic spatial resolution of 1.0 m to achieve a highly detailed representation of atmospheric dynamics. To ensure realistic inflow conditions for the core study area, two additional nested model domains were configured with progressively coarser isotropic resolutions of 5 m and 20 m. These domains provided the necessary boundary conditions for the high-resolution simulations while maintaining computational efficiency. The simulations were conducted using the PALM model (23.10) (Maronga et al., 2015, 2020), an LES model that solves the Navier–Stokes equations by directly resolving large-scale turbulence and parameterizing subgrid-scale turbulence. To study atmospheric flows, temperature, and humidity in an urban setting, the urban application module PALM-4U (Maronga et al., 2020) was used. The PALM-4U setup integrates realistic topographical spatial information and allows time-dependent steering of synoptic forcing conditions. The synoptic forcing conditions for the modeled simulation were derived from daily radiosonde data provided by the DWD station in Oberschleißheim, located north of Munich. Topographic and building data derived from the Bavarian Survey Administration (Vermessungsverwaltung, 2024). The initialization and runtime module steer basic model operations and employ settings for input and output LES. Here a spinup time of 24 h was embedded to initialize adjustments between the surface, soil- and wall-layer temperatures to prevailing atmospheric conditions before simulation start (Maronga et al., 2019). A Land Surface Module (LSM) summarizes information about land-use data for which cartographic basis was provided by the Bavarian Survey Administration. A static driver covers the information of the LSM and consists of a multi-layer soil model, predicting soil temperature and moisture content, and a solver for the energy balance at the surface. A nesting module includes one root domain in 20 m resolution and two nested inner domains in 5 m resolution that covers the city core area of 2 km x 2 km and the respective street canyon in a one way nesting mode (see Fig. 3). An urban surface module simulates building surface interactions using a tile approach. It consists of a multi layer wall and soil model, predicting wall and soil temperature and moisture content (Maronga et al., 2019). A solver for the energy balance is applied to calculate the temperature of the surface and the skin layer for each urban surface tile individually. The synoptic forcing conditions at start are provided externally. Radiation is performed using the Rapid Radiative Transfer Model (RRTMG) model. For z-values greater than 500, the grid was stretched by a factor of dz(k+1) = dz(k)1:08. The inner domain is shifted by 4420 cells from the lower left corner in x-direction and by 2980 from the lower left in y-direction of the root domain. It is a quadratic shape of 400 x 400 x 600 pixels (see Table 2). Each pixel from each domain covers information about topography, coordinates, and land-use type according to PALM-4U classifications or building. For each surface element of the model grid, the equations for sensible heat, aerodynamic resistance, ground heat, thermal conductivity and latent heat flux are solved locally and respectively from the energy balance. The chosen resolutions were found to be representative values providing an optimal trade-off between accuracy, covering whole city districts and computational feasibility.

Table 2
Model domain setup showing the dimensions of root and inner domains (resolution, x-direction, y-direction, z-direction, z-height) and shifts for the inner and child domains (origin of lower left corner in Universal Transverse Mercator coordinates).

	Parent domain	Inner domain	Child domain	Unit
resolution	20	5	1	m
x-direction	500	400	300	pixel
y-direction	500	400	400	pixel
z-direction	64	600	160	pixel
z-height	2578	600	160	m
origin	677 024	681 444	E-UTM	
origin	681 444	5 531 006	N-UTM	

As LES model simulations were conducted after and in addition to the measurement campaign, the simulations were performed to (i) test the capability of the model to reproduce the measured flow effects inside the street canyon and (ii) expand the measured information for the simulated information to explain the underlying mechanisms. A comprehensive validation of PALM in a comparable urban setup was previously performed by Sungur et al., who evaluated single-point measurements, first-order moments, and the space–time variability of wind and scalar fields using multiresolution decomposition (Sungur et al., 2025). In that study, PALM reproduced the space–time variability well, although notable offsets occurred during nighttime conditions. Building on this earlier work, the present study extends the validation to TKE, friction velocity, and sensible heat flux. Similarities between the two studies include the model resolution according to the size of the root and inner domains. A key difference lies in the applied forcing: while Sungur et al. used synoptic forcing derived from mesoscale model output, the present study employs radiosonde-based forcing. For the current study, two different, 50-hour periods that are representative in capturing typical and rare flow regimes within the street corridor were selected. The simulation periods were selected based on a systematic classification of large-scale weather conditions during the summer

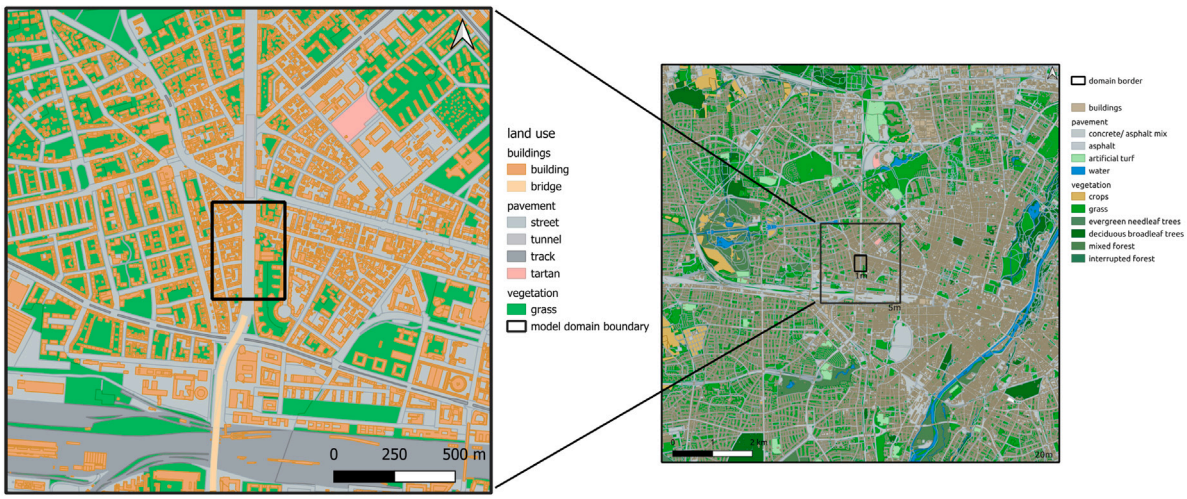

Fig. 3. Representation of the model domains in the LES model: (A) Schematic representation of the study area location. The colors indicate different land use types. (B) Nested domain approach of the study area (300 m × 400 m × 160 m) with a resolution of 1 m, first nested domain (2 km × 2 km × 600 m) with a resolution of 5 m, and parent domain (10 km × 10 km × 2630 m) with a resolution of 20 m.

months (May–October) of 2021 into distinct local airflow regimes. Two cases with stable and well-defined meteorological conditions – both in terms of local airflow and synoptic-scale weather – were chosen: (1) synoptic inflow from the west under cyclonic conditions (2021-07-20–2022-07-22), resulting in local northerly flow within the street canyon; and (2) synoptic inflow from the east under anticyclonic conditions (2021-09-07–2021-09-09), leading to local northwesterly and westerly flow within the street canyon. These distinct meteorological scenarios resulted in different effective flow directions and mixing intensities, particularly on the west side of the street canyon, where the air quality station and our experimental systems were located. As the AQS and the experimental setup are located on the western side of the street, they are directly impacted. Thus, simulations were expected to explain the pronounced contrast in the measured averaged NO_2 concentrations between the two airflow regimes. The flow metrics output is spatially discrete, derived from user-defined two-dimensional cross sections. The cross sections were strategically chosen to include multiple parallel north–south sections along the westbound and eastbound lanes, as well as west–east cross sections encompassing all measurement locations deployed during the field test.

Building upon the space–time variability validation presented by Sungur et al., the present study extends the model evaluation to turbulent quantities, including turbulence kinetic energy (TKE), sensible heat flux (Q_H), and friction velocity (see Section 2). Reproducing absolute magnitudes of turbulent quantities in urban large-eddy simulations (LES) remains inherently challenging due to unresolved microscale surface heterogeneity, anthropogenic heat flux variability, and measurement representativeness errors within the roughness sublayer. Nevertheless, the simulations realistically capture the characteristic diurnal evolution and the relative differences between synoptic west and synoptic east regimes. Observed wind speeds associated with the local north-flow regime – apart from rare strong southerly events – belong to the higher end of the measured distribution but generally remain weak, typically below 1.5 ms^{-1} (see Fig. 6). These low wind speeds reflect the orthogonal alignment of the street canyon relative to the prevailing synoptic forcing, resulting in reduced along-canyon momentum and limited mechanical turbulence production. The model reproduces these low absolute wind speeds and their vertical structure (Fig. 4b). Furthermore, the observed 180° wind-direction offset between synoptic west and synoptic east conditions (see Fig. 6) is consistently represented in the simulated vertical wind-direction profiles (Fig. 4c), indicating that the large-scale forcing is realistically translated into canyon-scale flow patterns. The comparison of simulated and observed turbulent quantities (see Fig. 5) demonstrates that the model adequately reproduces the overall diurnal cycle of TKE and (Q_H), as well as the relative differences between the two synoptic regimes. The largest discrepancies in absolute magnitude occur during the morning transition (see Figs. 5a–d), where the onset of turbulence appears delayed in the simulations. This shift is not attributable to inconsistencies between UTC and CEST but is likely linked to the representation of surface heating and boundary-layer growth in the model. In particular, for the synoptic east regime, simulated in September 2021, the delayed turbulence onset can be associated with seasonal differences in solar elevation angle and net radiation, which influence the timing and intensity of convective boundary-layer development. During nighttime, simulated TKE values are significantly lower than observations. This underestimation suggests that the model produces excessively stable stratification within the street canyon, suppressing mechanical turbulence production and turbulent transport. In reality, residual turbulence, intermittent shear-driven mixing, and unresolved local heat sources (e.g., anthropogenic heat release) may sustain higher nocturnal turbulence levels than represented in the simulations. Correspondingly, the simulated diurnal cycle shows a rapid decline of TKE after approximately 18:00 local time, consistent with the modeled decay of convective mixing following the reduction of surface heating. Finally, the standard deviation of observed turbulent quantities exceeds that of the simulations, reflecting the higher temporal variability and stochastic nature of real atmospheric turbulence compared to the more idealized and controlled boundary conditions imposed in the LES framework.

2.4. Traffic dynamics

The City of Munich operates numerous traffic counting stations, including one located within the study area. This station features eight double inductive loops, or 8+1 detectors, which continuously record traffic volumes and speeds while classifying vehicles into eight categories: motorcycle, passenger car, passenger car with trailer, van, bus, truck, truck with trailer, articulated lorry, and an additional "not classifiable" category. Resolution at 15 and 60 min aggregated traffic data, including volumes and average speeds, were obtained from the City of Munich's Mobility Marketplace. Emission factors were determined using the Handbook of emission factors for road transport (HBEFA) methodology, which incorporates traffic quality, road gradient, and pollutant class distribution as input parameters (INFRAS, 2019). The pollutant class distribution was determined through two number plate

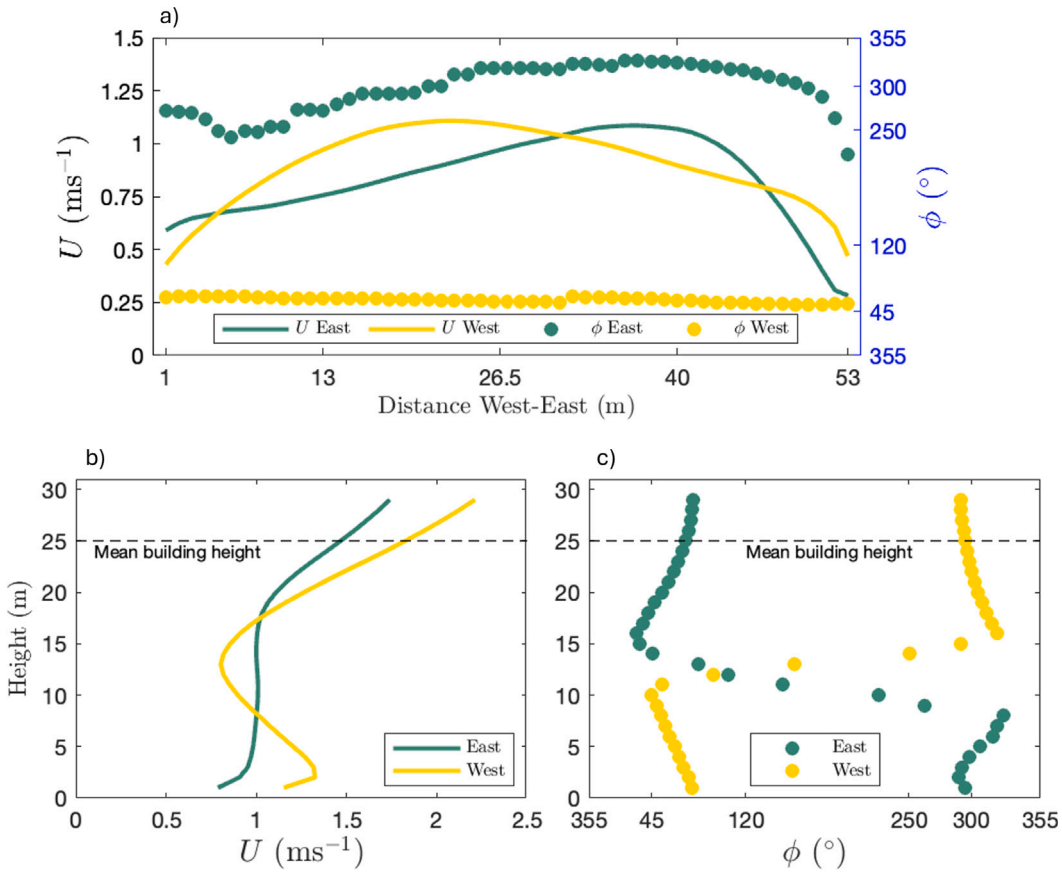

Fig. 4. Simulated wind characteristics under synoptic west (yellow) and synoptic east (green) forcing: (a) absolute wind speed as a function of wind direction regime, (b) horizontal wind speed profiles, and (c) horizontal wind direction profiles across the street canyon. The dashed line represents the mean building height.

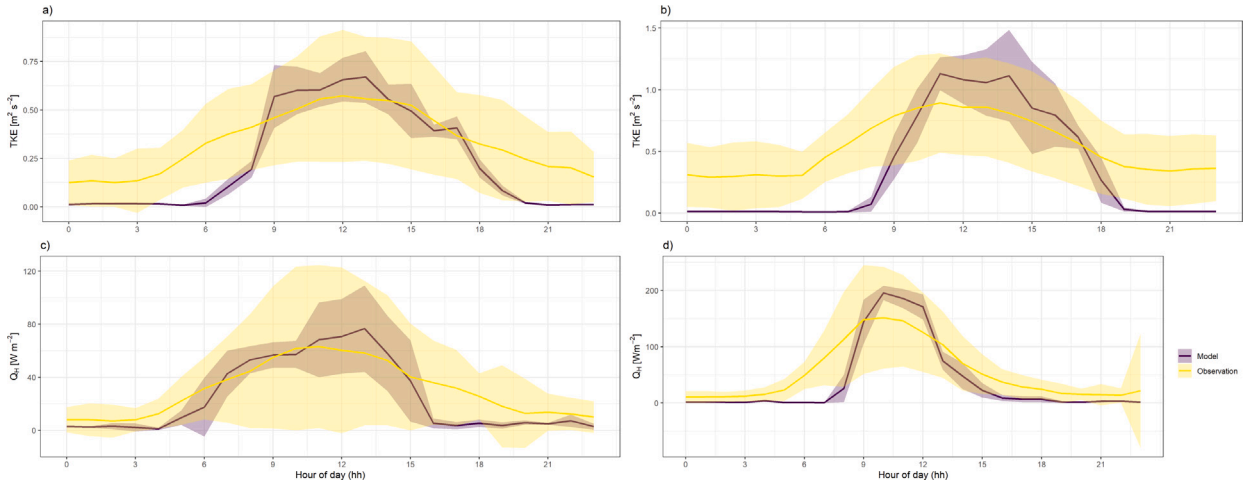

Fig. 5. Simulated and observed mean diurnal cycles of turbulence kinetic energy (TKE) and sensible heat flux (Q_H) for (a) synoptic west TKE, (b) synoptic east TKE, (c) synoptic west Q_H, and (d) synoptic east Q_H. For the simulations, the mean diurnal cycle is calculated from the two simulated days for each synoptic regime. The observational mean diurnal cycle is derived from weekday data collected between July 2021 and June 2023. As the simulations represent weekday conditions, only observed weekdays are considered for comparison. Colors distinguish model results (purple) from measurements (yellow). Shaded ribbons indicate the respective standard deviation mean diurnal cycle.

samples detected with automatic number plate recognition devices on two Tuesdays in the summers of 2021 and 2022. These were anonymously evaluated by the German Federal Motor Transport Agency. The HBEFA methodology distinguishes between five levels of service, based on the US "Highway Capacity Manual", which considers variables such as average speed, maximum permitted speed, and road gradient (Transportation Research Board, 2010). Accurate classification of vehicle types is critical for reliable emission calculations. The resulting emissions were calculated by multiplying the emission factors by the distance traveled and the traffic volume for each class of vehicles.

3. Results and discussion

To characterize the persistent elevation of the concentrations of NO_2 measured by the air quality station within the investigated street canyon, we analyzed the relative contributions of dynamic transport processes, traffic emissions and photochemical conversion to a concentration of NO_2 within the road corridor. Our long term analysis mentioned in 2.3 detected a statistically insignificant dependence between the synoptic forcing and the local street canyon flow regime. Since both short-term turbulent mixing and mean advective airflow significantly influence ground-level NO_2 concentrations in high-traffic street canyons bordered by tall buildings, we start by identifying dominant flow regimes and for each of those, analyze turbulent mixing processes, the latter of which are characterized using turbulent kinetic energy and sensible heat flux. We then assess the impact of turbulent mixing processes on the distribution of NO_2. In addition to meteorological parameters, traffic statistics within the street canyon are analyzed the latter to investigate how atmospheric conditions affect traffic dynamics and, consequently, pollutant emissions.

3.1. Air flow regimes

Our results show that the investigated wind direction at the long term measurement station of the street canyon is decoupled of large-scale synoptic forcing (see Fig. 6). Furthermore, the synoptic surface-flow direction measured at the DWD station, is not uniquely correlated with the General Weather Pattern (see Fig. 8). The longitudinal alignment of the street canyon, along with its bordering buildings, follows a north–south orientation and is orthogonal to the prevailing westerly flow in Central Europe. The wind field in the study area was classified into five effective airflow sectors based on directional frequencies.

- **North (355°–45°):** 44% frequency
- **Northwest (300°–355°):** 21% frequency
- **West (250°–300°):** 5% frequency
- **South (120°–250°):** 18% frequency
- **East (45°–120°):** 12% frequency

The most frequent airflow direction in the study area is local wind flow from the north (44%), with occasional occurrences of westerly flows (21% + 5% = 26%). Easterly flows occur less often, while southerly flows exhibit the greatest variability in wind direction which we prescribe to storm events captured in February 2022. For southerly flow, airflow occurs predominantly during night (see Fig. 6). The change between daytime northern flows and nighttime southern flows can be attributed to a mountain-valley breeze circulation in mountainous regions. As the city of Munich is located in the outwash plain of the alps, it is influenced by the alpine pumping (Graf et al., 2016). The near-surface mean airflow in the street canyon of differs significantly from that at the city's meteorological reference station which captures the synoptic forcing condition (see Fig. 6). Near-surface wind in the street canyon often flows opposite to the synoptic wind, with a notable 180° offset under westerly and easterly synoptic conditions. Northerly canyon flow prevails independent of the synoptic flow direction when the larger-scale synoptic forcing wind is weak (see Fig. 6). The observed reversal of the direction of near-surface airflow in the street canyon relative to synoptic flow above the urban canopy is explained by the results of the LES simulation 7.

Two distinct airflow regimes have been investigated, each exhibiting differences in atmospheric flow and transport processes, resulting in varying NO_2 concentration levels within the street canyon. In the following, we describe the synoptic forcing conditions for (i) westerly and (ii) easterly flow. To distinguish between the city-scale synoptic forcing and the airflow occurring within the street canyon, we refer to these as synoptic flow and local airflow, respectively.

3.2. Synoptic westerly flow

Under common prevailing large-scale synoptic westerly flow conditions, a stationary cross-canyon vortex reverses of the direction of airflow near the surface (see Fig. 7). A recirculation zone with TKE minima and dispersion is formed at ground-level on the west side of the street, corresponding to the location of the air quality measurement station. While air is transported from north to south within the street canyon, the near-ground flow comes partially from north and east, meaning that air is first transported across the street canyon before it arrives at the air quality station. Our findings contradict the expected dependency between the street canyon flow regime and the overarching synoptic patterns. Although the interaction between wind and urban obstacles is inherently complex, typical flow regimes in urban environments can be well studied and understood when the above-roof flow is perpendicular to the canyon. A factor of 2 between width and street height and an orthogonal course of the investigated street canyon to the synoptic regime leads to the assumption of wake-interference and cross-canyon vortex flow. The canyon's aspect ratio (AR), i.e. the ratio of building height to street width (AR = 1:2.5), is with AR = 0.4 particularly wide. Thus, the downwind building disturbs the flow before readjustment can take place, expected to be a "wake interference" flow (Chung and Liu, 2013; Xie and Huang, 2007; Hunter et al., 1992). In this suggested wake interference regime, the friction factor decreases with increasing aspect ratio. The prevailing airflow does not touch down to the ground and the flow only partly entrains into the upper street canyon, and the ground-level separation diminishes instead (Chung and Liu, 2013). However, simulation results showed only one vortex in the street canyon. The stationary vortex shown in our simulation (see Fig. 7) of the street canyon, supports the assumption that a wake-interference flow, characterized by a rotational cross-canyon vortex, developing in the wake zone of the windward-facing building (Oke et al., 2017). A shear zone develops which accelerates the top layer of the canyon air and consequently a strong re-circulating eddy, but the size and extent of eddy is controlled by the height difference of the buildings and specifically height of the leeward building. In dense urban environments, the predominant wind directions are often dictated by the alignment of the street network. The wind field is substantially altered by the surrounding streets and buildings in the immediate vicinity of the local measurement station. Therefore, the north wind predominates in the north–south oriented street canyon.

Side streets entering the study area from the west were found to systematically induce the north–south directed streamline of the street canyon (see Fig. 8). In combination with the presence of a stationary vortex, this organized turbulent behavior significantly modulates the near-surface airflow. LES results reveal a dominant near-surface northerly component at the AQS, shaped by both the influence of side-street inflow and building-induced vertical structures (see Fig. 8). The presence of side streets introduces additional perturbations, enhancing local turbulence and potentially reinforces the development of a counter-rotating vortical structure. They create significant cross-canyon flow (spanwise flow and mixing), which persists for about 10–25 meters depending on the side-street location in the flow direction by advective transport of TKE. While the width of the northermost side-street is largest and of another angle, the other side-streets are very much alike in their geometry (see Fig. 2). A systematically spatially larger cross-canyon flow is observed for the northern side streets compared to their southern counterparts. All side street air flow entries break up the vortices (see Fig. 8), but then the expected flow regime reestablished quickly. In between the side-streets, a wake interference flow along the north–south axes can be detected, building a counter-rotating vortical structure of airflow parcels with flow opposite to the prevailing flow. The simulated wind direction exhibits an approximate 20° eastward deviation compared to in-situ measurements, suggesting

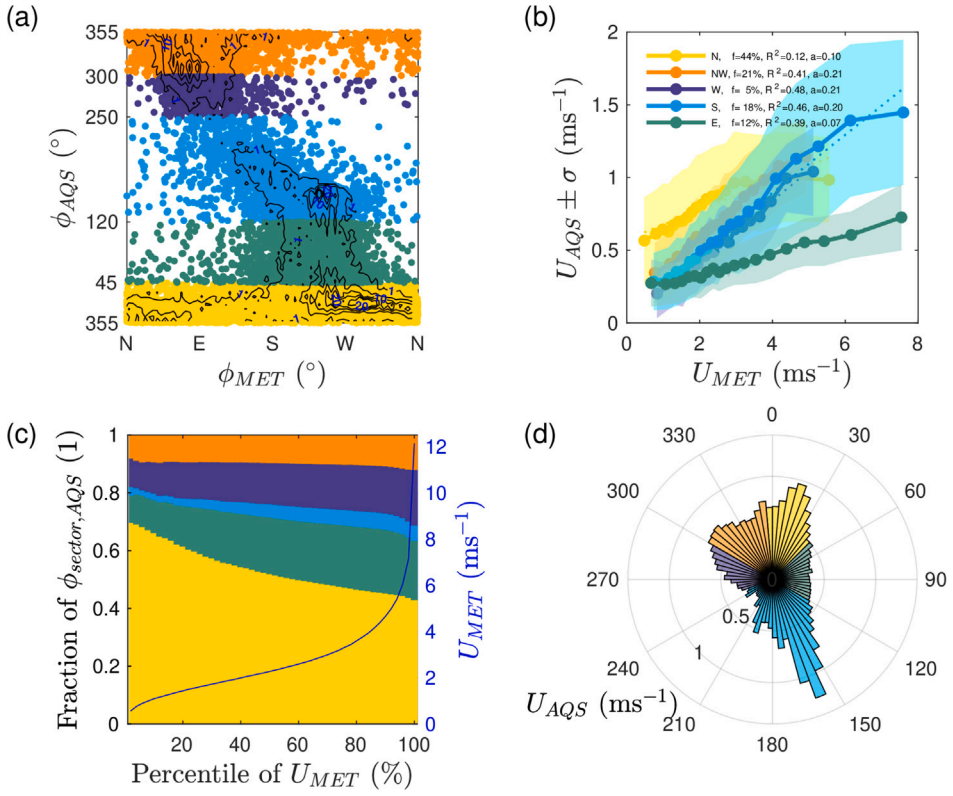

Fig. 6. Measured mean airflow statistics at the street canyon. Comparison of (a) mean wind directions (°) and (b) wind speeds (U) and standard deviation at the AQS within the street canyon with those at the reference station (MET); (c) distribution of fraction of wind direction sectors (y-axis) at the AQS station as a function of percentiles of wind speed U (x-axis) and wind speed U (z-axis) at the reference station (MET); and (d) wind speed (U) distribution relative to wind direction at the AQS station. The observation period spans from July 15, 2021, to September 15, 2023.

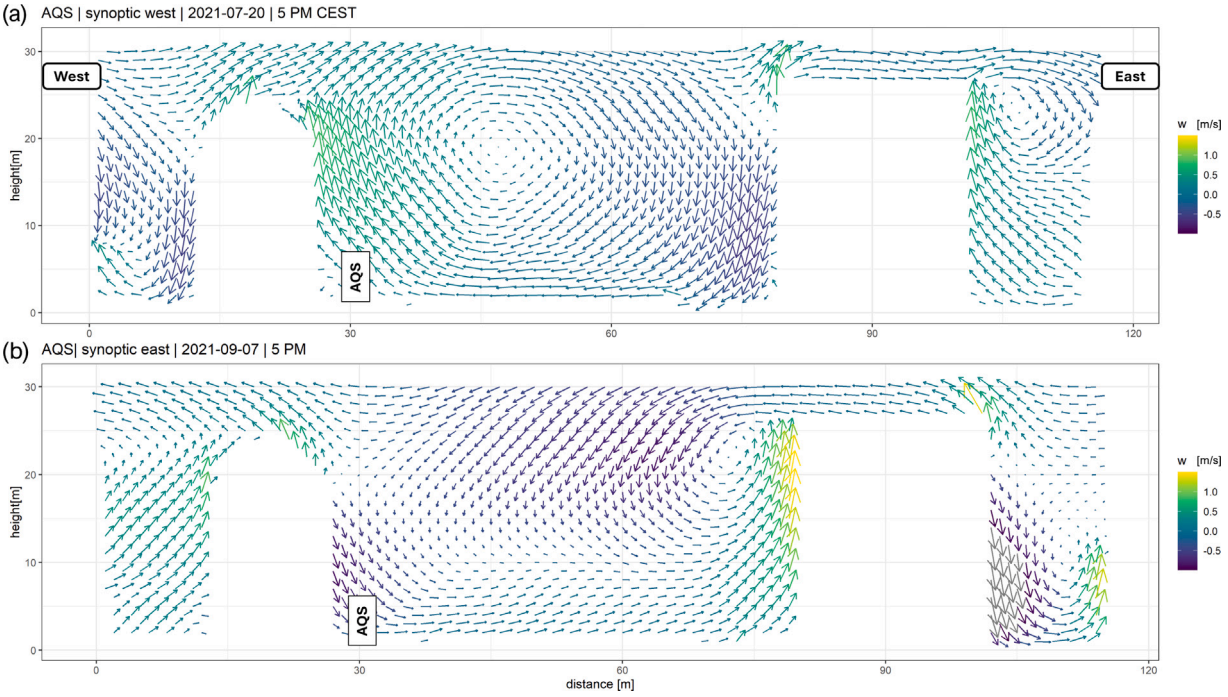

Fig. 7. Cross section in west-east direction of the street canyon width showing u (arrows) and w (color range) streamlines at the location of the Air Quality Station (AQS) within the studied street canyon length. The cross section was taken at 5:00 PM CEST. White spaces symbolize buildings on the western and eastern side of the street canyon.

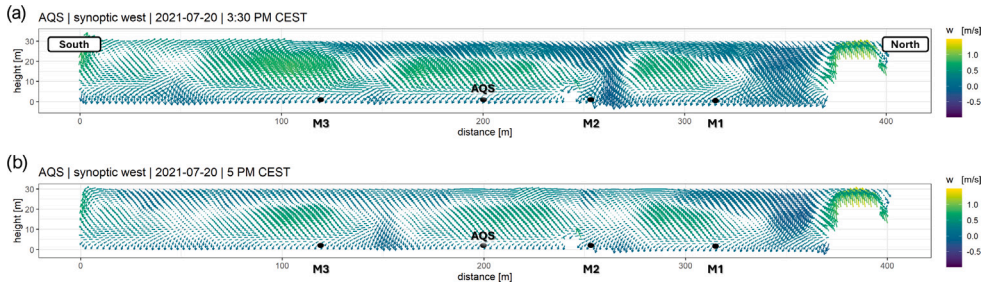

Fig. 8. Simulated 30-min mean streamlines of airflow in the longitudinal section of the study area around the AQS (within a 200 m distance), shown as an example under synoptic westerly flow conditions on July 20, 2021, at 3:30 PM (a) and 5:00 PM (b) Central European Summer Time. M1- M3 represent the comparative measurement locations. Sidestreets are located at 150 and 260 m distance shown by the *y*-axis of the graphic. The streamline flow is depicted by u (arrows) and w (color range).

potential discrepancies arising from model resolution, boundary conditions, or simplifications in the representation of urban geometry. Given that the simulated wind directions and velocities are closely aligned with observational data, the representation of a single dominant vortex in the model appears to adequately capture the key dynamics of canyon flow in this configuration (see Fig. 7). Simulated streamlines in the longitudinal direction reveal the presence of four turbulent vortices forming between the side streets located to the west. The vertical velocity component increases within each vortex, with the vortex centers positioned south of each side street (see Fig. 8). The location of the AQS, in relation to the additional measurements at site M2, indicates exposure not only to streamflow in the west–east direction but also in the north–south direction. The vertical velocity component at the AQS is nearly zero, suggesting predominantly horizontal air transport—likely carrying higher pollutant concentrations from the dense road traffic.

3.2.1. Wind speed characteristics

The orthogonal orientation of the street canyon relative to the synoptic flow, combined with the high surface roughness of the surrounding building infrastructure, leads to a significant reduction in wind speed at the local air quality station compared to the reference station 3.1 d. Wind speeds in street canyons are highly dependent on the orientation of the respective street canyon to the prevailing direction of synoptic flow and can thus lead to both an increase or decrease in wind speeds (Oke et al., 2017). Orthogonal synoptic flow typically reduces wind speeds within the investigated street canyon. For local wind directions from the north and east, wind speeds are reduced to 7%–10% only, of those measured at the reference station, whereas for all other local directional sectors, wind speeds reach approximately 20% of those measured at the reference station (see Fig. 6(c)). The wind speeds occurring for local north and south airflow regimes are the highest in absolute terms but remain relatively low, with values typically below 1.5 ms^{-1} (see Fig. 6). The weak northerly wind flow measured at the AQS may also point to vehicle-induced air movement, as the AQS is located on the western side of the street canyon. Consequently, vehicle motion from north to south generates within-street-canyon airflow that is detected as northerly wind at the measurement site when the canyon flow is weak. We undergo further investigation and explanation in 3.4.1.

3.3. Mixing intensity contribution

The mixing intensity, represented by the turbulent kinetic energy (TKE), exhibited a clear dependence on the direction of the wind measured at the air quality station (see Fig. 9 a)). Normalized TKE per unit generalized momentum flux was weakest for the most common weak wind north flow regime during synoptic westerly forcing (see Fig. 9 b)). As weak wind speeds cause weak turbulent mixing intensities, we attribute low TKE values to low absolute wind speeds caused by the orthogonal alignment of the street canyon. At the crossing of each side street, higher TKE mixing is observed (see Fig. 15) for the synoptic west condition only. In the investigated street canyon aligned approximately orthogonal to the synoptic wind direction, the along-canyon flow is weak and characterized by a recirculation cell with low mean velocities and reduced TKE. Under these conditions, turbulence production by shear is limited, resulting in weak mixing and pollutant accumulation. The recirculation zone thus results in a low intensity of turbulence and reduced mixing, leading to a pronounced accumulation of traffic-related emissions. At street intersections, however, this quasi-steady recirculating flow is locally disturbed by inflow from the orthogonal side streets (see Fig. 15). The velocity difference between the weak recirculating canyon flow and the incoming side-street flow increases the local velocity gradient leading to enhanced horizontal but also vertical shear, thereby enhancing shear production of TKE. The intersections act as localized turbulence generation hotspots as they introduce additional momentum. Thus, within an overall low-mixing regime, spatial heterogeneity in turbulence arises from geometrical discontinuities such as crossings. The unusually high TKE observed in the southern sector for wind directions ranging from 150° to 170° was attributed to nocturnal storm conditions in February 2022 (see Fig. 9). During this period, the synoptic inflow direction was aligned with the longitudinal axis of the street canyon, resulting in significant shear-induced turbulence. This is regarded and treated as an extraordinary event not representing the common flow regime.

3.4. Sensible heat flux

Turbulent mixing of air transports heat and moisture, typically away from the surface. The resulting fluxes of sensible and latent heat are primarily driven by turbulence, including a smaller contribution from transport by mean motion. The turbulent sensible heat flux is related to the logarithmic profile of the temperature. Across the northwest, west, and north sectors, the relative sensible heat transport causes the TKE to exhibits a distinct diurnal variation (see Fig. 9c), driven by surface warming due to absorbed solar radiation. A positive flux up to 0.2 K ms^{-1} is measured at the air quality station, indicating limited upward heat transport during the day. Simulations using the LES model also show variation in the magnitude of turbulent sensible heat flux depending on the large-scale synoptic forcing (see Fig. 17) particularly between synoptic westerly and synoptic easterly flow conditions. Under westerly synoptic flow, the simulated sensible heat flux exhibits a clear diurnal cycle, peaking at 0.25 K ms^{-1} around 14:30 pm. However, variation of the amplitude is high and the cycle time is very low as daytime flux values before 12:00 am and past 14:30 pm stay below 0.1 K ms^{-1}. Near-zero values observed during nighttime. In combination with the measured low TKE, this leads to a stabilization of the air as a result of air density effects. Such stabilization further suppresses turbulent mixing and reduces turbulent exchange.

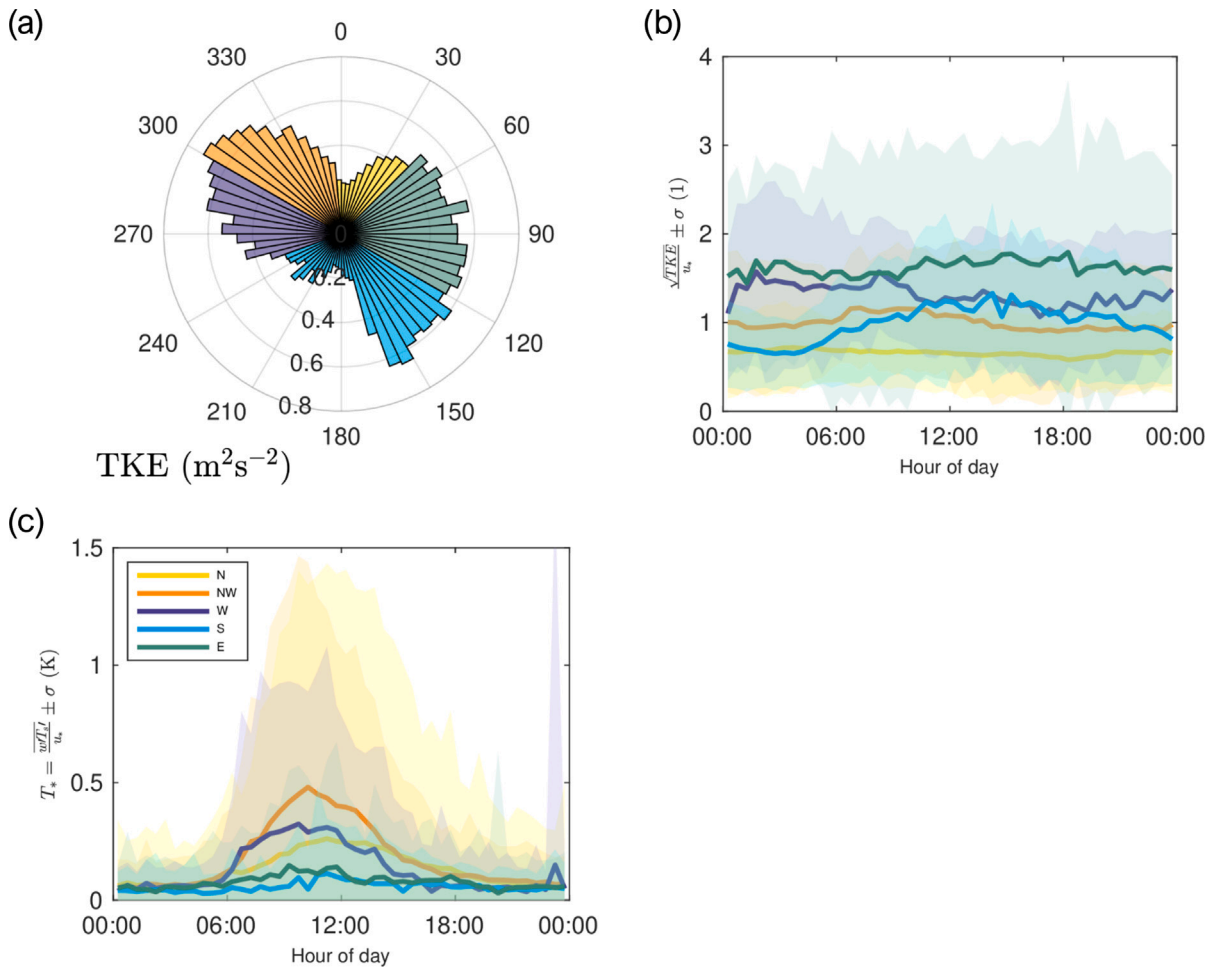

Fig. 9. Measured mean turbulence statistics of the airflow at the AQS. (a) Distribution of TKE as a function of wind direction, (b) Dimensionless mixing intensity represented as the ratio of TKE to shear stress velocity (u), and (c) Relative heat transport expressed as the ratio of sensible heat flux to shear stress velocity. The observation period spans from 07-15-2021, to 09-15-2023.

3.4.1. Vehicle induced turbulence

Given the exceptionally weak wind conditions combined with extremely high traffic volumes in the street canyon this study investigates the expectation whether vehicular motion itself has a measurable influence on near-surface airflow and, by extension, on turbulent mixing processes. An analysis of vehicle traffic data on the eight-lane roadway indicates that day of the week and time of day are the primary predictors of traffic patterns, with minimal influence of seasonal variation (see Fig. 10). Clear traffic peaks are between 6:30 and 9:00 AM in the morning hours for weekdays only and 4:00 - 6:00 PM in the afternoon hours for weekdays and weekend days. Traffic peaks can be clearly recognized when analyzing the hourly travel speed (see Fig. 10(b)) which is lowest for times during traffic peaks, especially during the afternoon traffic peak. With traffic peaks reaching up to 10,000 vehicles per hour, it is plausible that vehicle movement contributes to a lane-dependent baseline flow. In addition, the release of thermal energy from predominantly combustion-engine vehicles may drive buoyancy effects that further enhance vertical mixing. To explore this, we integrated meteorological, air chemistry, and traffic datasets to evaluate causal links between traffic activity and turbulence generation.

The street canyon airflow from the north is associated with poor ventilation. Turbulence kinetic energy, measured at the air quality station via ultrasonic anemometry, shows a strong linear correlation with both vehicle counts and the product of vehicle count and speed, up to a threshold of 0.63 to 0.65 ms^{-1} as depicted in Fig. 11. TKE is expressed as the square root of its standard form to normalize its quadratic dependence on velocity, thereby enabling a simplified linear relationship. The results show that the linear correlation remains consistent regardless of the day of the week or the time of day (see Fig. 11). This indicates that vehicle movement itself mechanically generates turbulence and enhances mixing. This approach introduces a parsimonious explanatory framework for turbulence generation under weak-wind, high-traffic conditions, offering a novel and data-efficient method for assessing traffic-induced turbulence in urban street canyons. Therefore, it is highly likely that the airflow from north on the western side of the street canyon is impacted by the southward movement of vehicles. We therefore expect statistical independence of atmospheric TKE and vehicle-induced TKE only, when atmospheric TKE intensifies due to meteorological conditions and exceeds the threshold values of 0.63 to 0.65 ms^{-1}. In forcing regimes where TKE is rather low, VIT thus becomes significant. Still, we cannot exclude the influence of other forcings. The ratio of atmospheric TKE to vehicle-induced TKE exhibits a pronounced diurnal variation, as both wind shear and buoyancy-driven turbulence are influenced by solar radiation and the resulting pressure differences throughout the day (see Fig. 11).

3.4.2. Dispersion of NO_2

To characterize the mean concentrations of NO_2 in the study area, daily variations were derived from the mean values measured at 30-minute intervals for the characteristic airflow regimes (see Fig. 13). Our results show no characteristic seasonality. The daily minimum occurs in the early morning around 03:00–04:00 CEST. After this minima

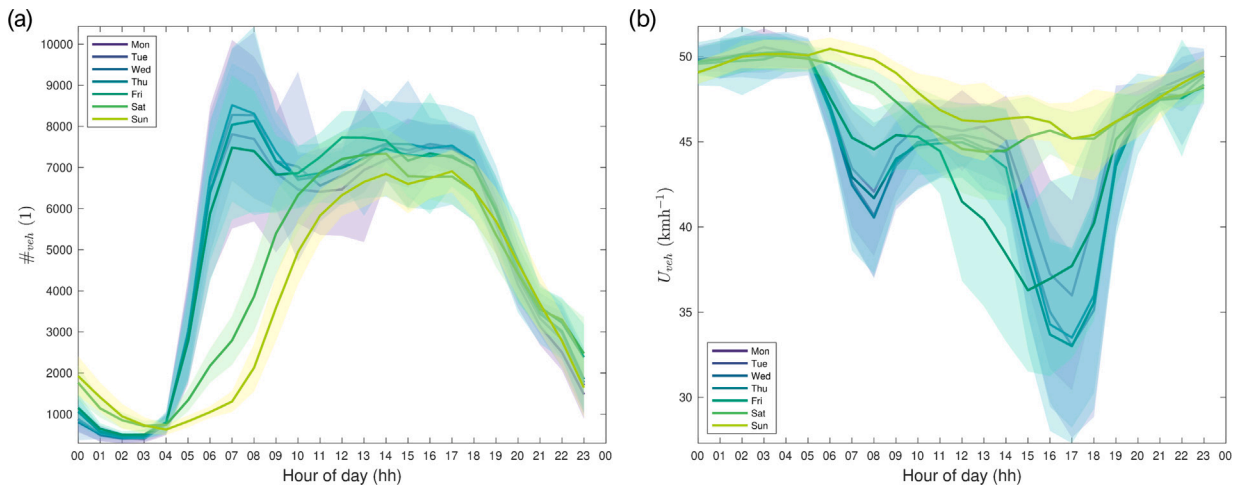

Fig. 10. Mean daily variation of the number of vehicles per hour (#veh, left) and the hourly travel speed (U_{veh}, right) at the investigated street canyon at the height of the AQS, categorized by day of the week during the study period from 15 July 2021 to 20 June 2023. The mean value with a ribbon of the standard deviation is presented.

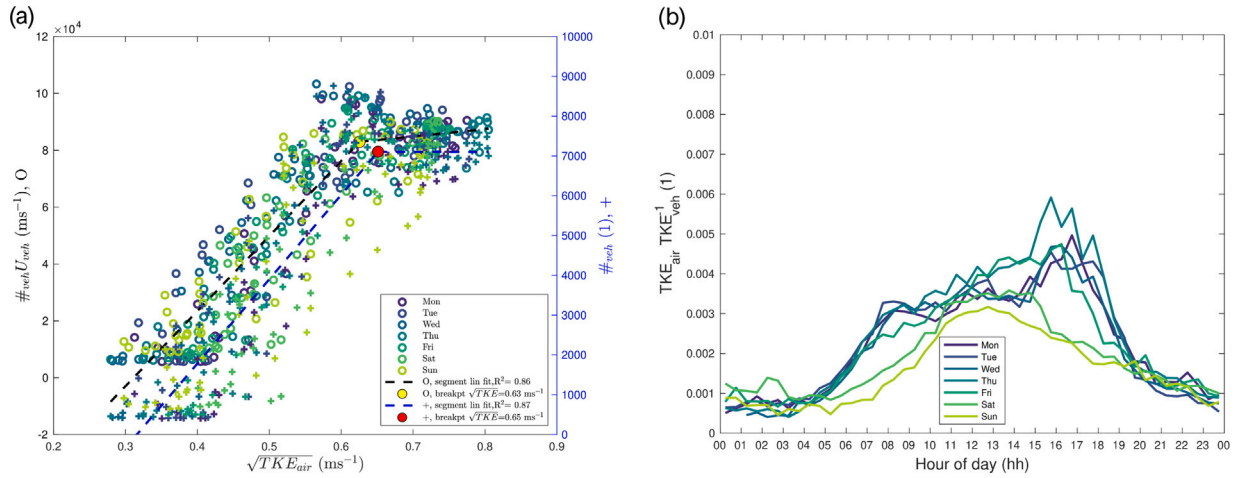

Fig. 11. Relationship between atmospheric mixing and traffic dynamics for the *N* and E sectors. (a) Mean number of vehicles per hour (#*veh*) and the product of vehicle count and driving speed (#*veh x* U_{veh}) plotted against mean turbulent kinetic energy (TKE). (b) Ratio of measured atmospheric TKE to traffic-induced TKE. Segmented linear models with breakpoints are included. Results are presented separately for each day of the week but encompass all times of day. The study period was from 07-15-2021 to 09-15-2023.

the concentrations increase across all flow regimes in response to the increasing traffic volume. The measured concentrations of NO_2 are expected to be primarily influenced by traffic dynamics, as road traffic serves as a primary and secondary source of NO_2 (Amato et al., 2013). Based on the high variance of results, we conclude that significant differences in turbulent mixing and mean air transport in dependence on the airflow regime have a major impact on the measured concentrations of NO_2. On average, elevated mixing ratios NO_2 persist throughout the day, gradually decreasing after 18:00 or 19:00, depending on the prevailing airflow. This diurnal variation is characteristic of urban environments and closely follows traffic patterns. Our results have shown clear traffic peaks between 7:00 and 9:00 AM and 5:00 and 6:00 PM (see 10). In the case of the statistically most present northerly flow inside the investigated street canyon, high NO_2 concentrations are reached as the flow direction from north to south transports NO_2 rich air inside the tunnel out to the street canyon and directly to the measurement station before it is mixed upward with the air from the street canyon. Therefore measured NO_2 concentrations show highest concentrations of all airflow regimes at the air quality station and mobile CAPS locations. On average, NO_2 concentrations of 47 ±23, 42 ±23, 42 ±21, and 34 ±15, μgm^{-3} were measured by CAPS as mean values of 30 min at AQS and sites 1, 2 and 3, respectively. The relative standard deviation is high, approximately 50%, highlighting the substantial variability of NO_2 concentrations close to the emission source.

The highest average concentrations, which peak at 72 μg m^{-3}, occur in the afternoon hours for the local northerly airflow regime. The local flow from the South sector, which is characteristic for this inflow sector during nighttime hours, occupies an intermediate position in the mean daily NO_2 concentrations. The national standard limit value of 40 μg m^{-3} is consistently exceeded, except during the night hours between midnight and approximately 03:30 13. A statistical correlation between mixing and traffic dynamics also suggests a link to the measured NO_2 concentrations. The ratio of the measured NO_2 concentration to the NO_2 emissions exhibits a linear dependence on the linearized turbulent mixing intensity (TKE), indicating that the primary process governing NO_2 concentrations is the dilution of traffic emissions through turbulence. The ratio of measured NO_2 concentration to NO_2 emissions, derived from vehicle fleet composition using the HBEFA method, represents the fraction of emissions that persist as immissions in the street air and are thus potentially harmful to health (Anenberg et al., 2022; Costa et al., 2014, 2020). In particular, vehicle-induced mixing contributes

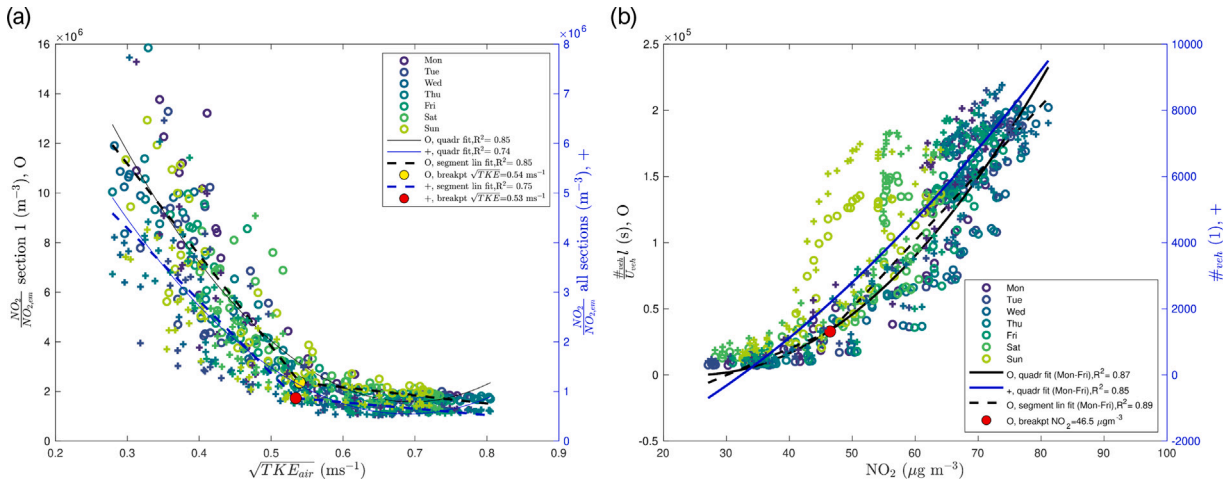

Fig. 12. Relationship between NO_2 concentrations, emissions, turbulent mixing, and traffic dynamics for inflow from the north and east sectors. (a) Ratio of measured NO_2 concentration to calculated NO_2 emissions as a function of mean TKE for the road section with a gradient. (b) Constructed statistical dimension "vehicle seconds", derived from the number of vehicles ($\#veh$) divided by vehicle speed (U_{veh}) and multiplied by the road section length, compared to the mean measured NO_2 concentration at the AQS. Results are presented separately for each day of the week but include all times of day. The study period was from 07-15-2021 to 09-15-2023.

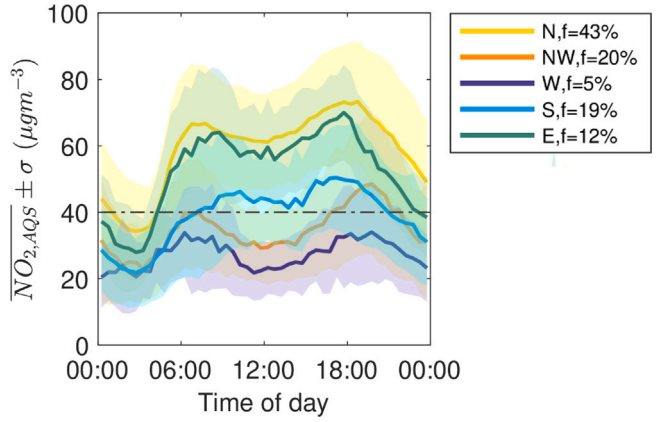

Fig. 13. Mean daily variation of NO_2 concentrations measured at the air quality station for the five airflow sectors during the study period from July 15, 2021, to September 15, 2023.

to a reduction in the fraction of NO_2 retained as immissions. This mechanism implies that increasing traffic density paradoxically leads to a relative decrease in the effective NO_2 load per unit of emission due to enhanced turbulence (see Fig. 12). This finding has a dependency with the time of the day, traffic peaks between 06:00 - 07:00 am CEST and 04:00 - 05:30 pm CEST. However, since total emissions increase drastically with increasing vehicle numbers, the absolute NO_2 concentration still increases despite the enhanced mixing.

3.4.3. Synoptic easterly flow

Synoptic easterly flows are rare in the study area, but since they are associated with the lowest NO_2 concentrations in the street canyon, they provide valuable insights into our investigations of the interaction between aerial transport and air pollutants (see Fig. 6). However, synoptic easterly forcing conditions are of much interest, as we exhibit the most significant differences in NO_2 concentrations between the common flow regime from synoptic west 13. Furthermore, we expected flow regimes of synoptic west and synoptic east to show clear contrast in exchange behavior of air and energy at local scale within the investigated street canyon. When comparing the measured wind direction of the street canyon with the measured wind directions at the city-wide reference station, a reversal of airflow predominantly between the synoptic east and local west sectors is shown (see Fig. 6). The LES results provide a mechanistic explanation for the observed airflow reversal depicted in Fig. 6(a). Under synoptic easterly flow conditions, a stationary cross-canyon vortex develops, exhibiting a recirculation pattern opposite to that observed during synoptic westerly conditions. This results in a reversal of the near-surface airflow direction within the canyon—from westward to eastward (see Fig. 7). In this configuration, fresh air originating from the east above the canyon is advected towards the western building facades and entrained into the vortex near the location of the AQS. The vortex extends further over the surface of the high-traffic street, subsequently mixing with the fresh air aloft above the canyon. Thus, synoptic easterly flow induces downdrafts of relatively fresh, unpolluted air which are transported from the northwest and west towards the AQS station, following the westerly flow along the street canyon. For the synoptic east conditions case, the advantages of the rather highly separated buildings of the street canyon come into play that generate much interaction with clean air as expected from fundamental mechanisms controlling dynamics in urban street environments as exemplary depicted by Martínez-Sánchez et al. (2023). Results show that the center of the vortex shifts little by time. While the vortex is established concentric for synoptic western conditions, the center of the vortex for synoptic eastern conditions is located towards the eastern side of the street canyon. Thus the airflow from above the canyon mixes directly into the airflow which has traveled through the AQS towards the street and therefore is at constant exchange with non-pollutant air (see Fig. 7). This results in low pollutant concentrations and enhanced mixing in the area of the air quality station.

3.4.4. Wind speed characteristics

Fig. 6(b) indicates that wind speeds can reach up to 7 ms^{-1} under synoptic easterly flow conditions. However, these elevated synoptic wind speeds do not effectively penetrate the street canyon. Instead, the opposing flow induced within the canyon leads to significantly reduced wind speeds- approximately 1 ms^{-1} at the measurement site (see Fig. 6). Our results reveal a distinction between daytime and nighttime wind speeds, reflected in the u- and v-velocity components (|1.12| and |2.37|, respectively), which can be attributed to thermal differences, regardless of the prevailing flow direction. Daytime variation in wind speed within the street canyon remains little across all observed flow directions.

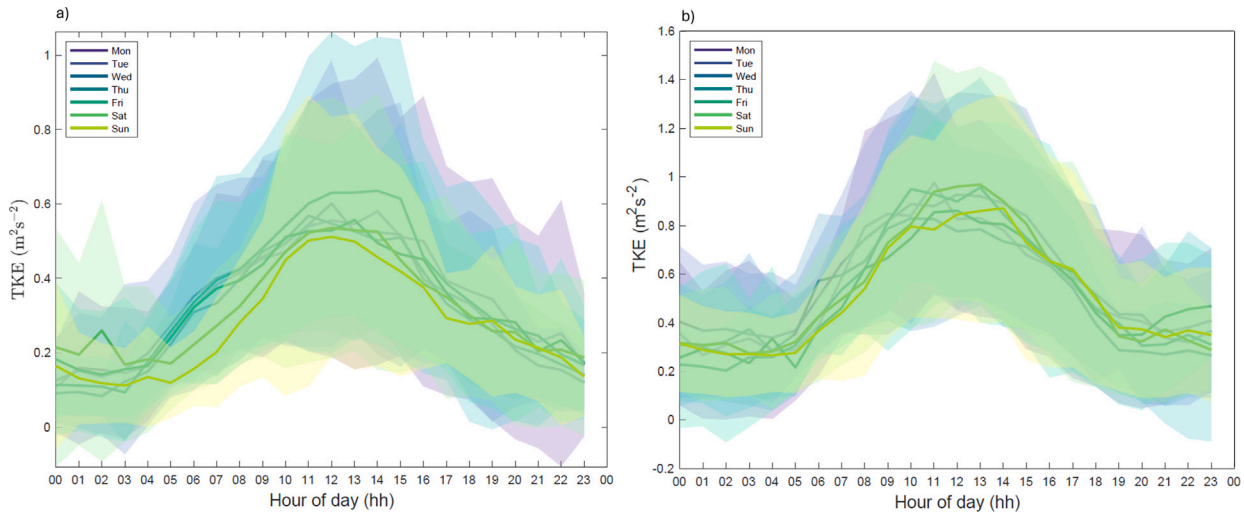

Fig. 14. Mean diurnal cycle of TKE for measured flow regimes: (a) North–Northeast and (b) West–Northwest, derived from observations at the AQS for the period July 2021–July 2023. Individual weekdays are distinguished by different colors in panels (a) and (b). The shaded ribbons represent the standard deviation associated with each weekday's mean diurnal cycle.

3.4.5. Mixing intensity contribution and vehicle induced turbulence

TKE values were highest for the measured Northwest and West airflow regimes (see Fig. 9). The high mean measured TKE between 0.5 and 0.6 $m^{-2}s^{-2}$ for the east sector can be largely attributed to the movement of vehicles along the eight-lane roadway. This effect is already explained in detail in Section 3.4.1. The impact of vehicle induced turbulence can be quantified when comparing the mean diurnal course from 2021-07–2023-06 for TKE between weekdays and weekend. While the Northeast and East sectors (synoptic west) show differences between weekdays and weekend, west northwest sectors (synoptic east) show a similar diurnal course of the day. We attribute the changes between weekday and weekend for the synoptic west condition to vehicle induced turbulence, as the vehicle fleet is significantly lower on weekends than on weekdays and thus vehicle induced turbulence does evolve less intensively for weekends. Effects of changes due to forcing regimes are not expected, as our analysis includes a mean taken over a period of almost two years (see Fig. 14). For the synoptic east conditions, TKE is past the threshold of 0.63 to 0.65 ms^{-1}. Like the results from observations, the modeled TKE at the air quality station is significantly higher compared to the low-exchange scenario associated with near-surface northerly flow (see Fig. 16). Mean modeled TKE values even reach up to 2.6 $m^{-2}s^{-2}$ with a clear peak at 14:30 for the simulation period at the location of the AQS. Fig. 15 shows elevated near-surface modeled turbulent kinetic energy (TKE) along the south–north cross-section at the air quality station (AQS), with spatially higher proportion of TKE within the street canyon under synoptic easterly conditions compared to synoptic westerly conditions.

Effects of side-street crossings on TKE differ substantially under this synoptic forcing regime compared to the synoptic west condition (see Fig. 15). The simulated longitudinal cross section reveals enhanced TKE throughout the street canyon rather than localized peaks at intersections. Modeled TKE values reach up to 2 ms^{-1} and exceed the magnitudes measured at the AQS. In contrast to the weak-wind regime, turbulence production is no longer primarily controlled by lateral shear at side streets. Instead, strong mechanical production above roof level generates elevated turbulence within the roughness sublayer, which is transported downward into the canyon. This top-down mixing mechanism increases the background turbulence intensity and spatially homogenizes TKE, thereby diminishing the relative impact of intersection-induced shear.

3.4.6. Sensible heat flux

The measured relative sensible heat transport for local Northwest regimes is, on average, 2 times higher in magnitude than in the north, south and east sectors (see Fig. 9c). The prevailing fluxes for local northwest and west regimes both show a much more pronounced diurnal variation. During low-cloud, anticyclonic weather conditions, intensified surface warming leads to greater heating of the air above (Liu et al., 2024; Steinfeld et al., 2020). The resulting decrease in air density facilitates upward motion, enhancing turbulent mixing and consequently promoting the dilution of ground-level NO_2 emissions from road traffic (see Fig. 17). The dependence of sensible heat flux on atmospheric mixing means that enhanced mixing not only results from but also reinforces increased vertical heat exchange, establishing a positive feedback between surface heating and turbulence generation. As a result, improved mixing and further promoting of turbulence contributes to lower pollutant concentrations. An pronounced sensible heat flux during noon throughout the entire simulated period was also observed for the synoptic easterly flow simulations, showing alignment with the local Northwest and West regime measured 17. This enhancement is particularly remarkable because the representative synoptic easterly forcing is based on September conditions, whereas the synoptic westerly case represents July conditions. Despite the seasonal reduction in solar elevation angle and shorter day length in September, the modeled sensible heat flux under easterly forcing exceeds that under westerly forcing. This indicates that the enhanced flux cannot be attributed primarily to seasonal differences in incoming shortwave radiation. Instead, the stronger sensible heat flux under synoptic easterly conditions is likely related to differences in boundary-layer structure and mesoscale forcing. E.g. reduced horizontal advection and subsidence-dominated background flow promote stronger local surface heating and a more pronounced development of a convective boundary layer. More effective vertical exchange between within the street canyon may allow buoyancy-generated turbulence above building height to penetrate downward. Consequently, buoyant production of turbulence dominates over shear-generated contributions, leading to enhanced vertical heat transport throughout the canyon despite the later seasonal timing.

Thus, the elevated sensible heat flux observed under synoptic easterly conditions reflects dynamically more favorable mixing conditions and boundary-layer instability rather than differences in solar forcing alone.

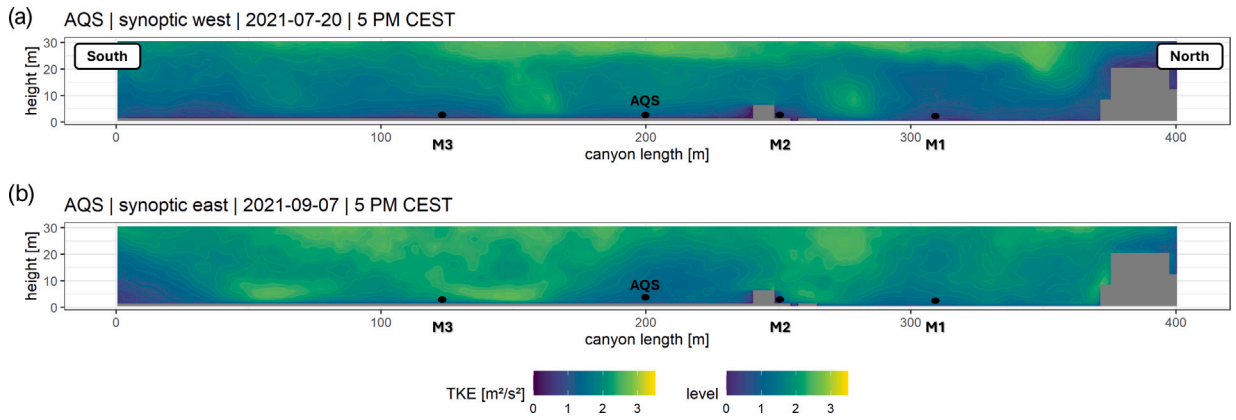

Fig. 15. Simulated TKE of the airflow at street canyon cross section from south to north. The cross section axis was taken at the location of the AQS and the graphic height is shown up to the street canyon height. (a) synoptical western flow, (b) synoptical eastern flow. The simulation was taken on (a) 2021-07-20 and (b) 2021-09-07.

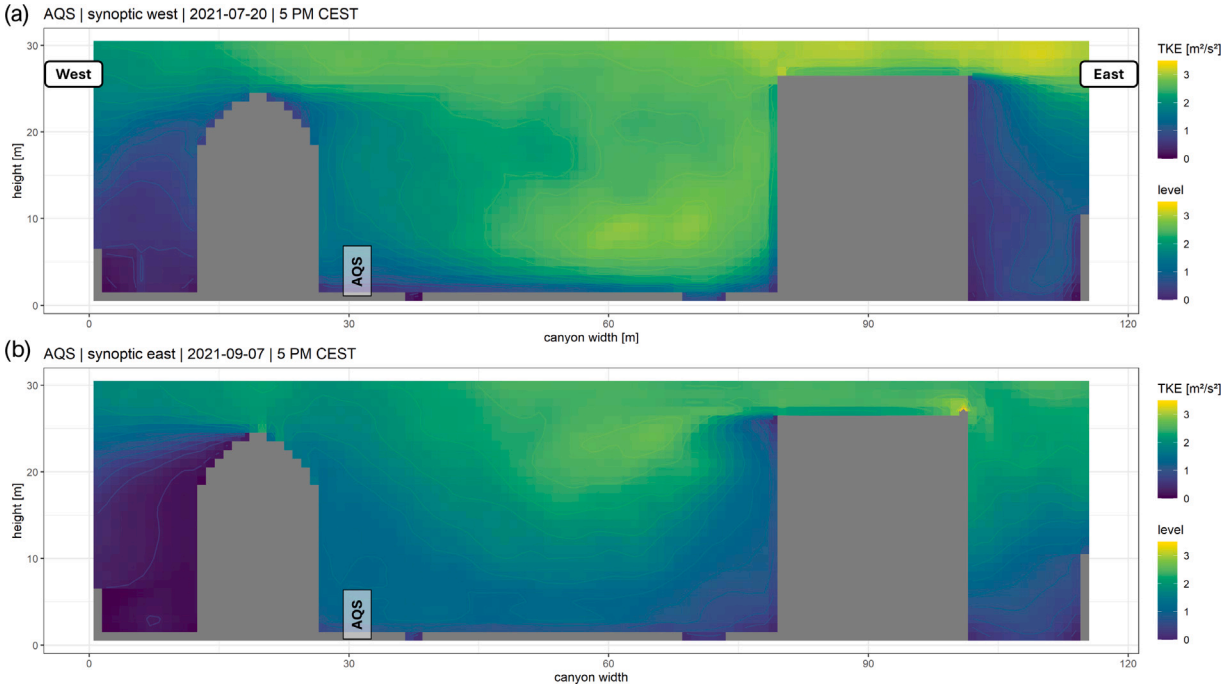

Fig. 16. Simulated TKE of the airflow at street canyon cross section from west to east. The location was taken at the AQS and up to the street canyon hight. (a) synoptical western flow, (b) synoptical eastern flow. The simulation was taken on (a) 2021-07-20 and (b) 2021-09-07.

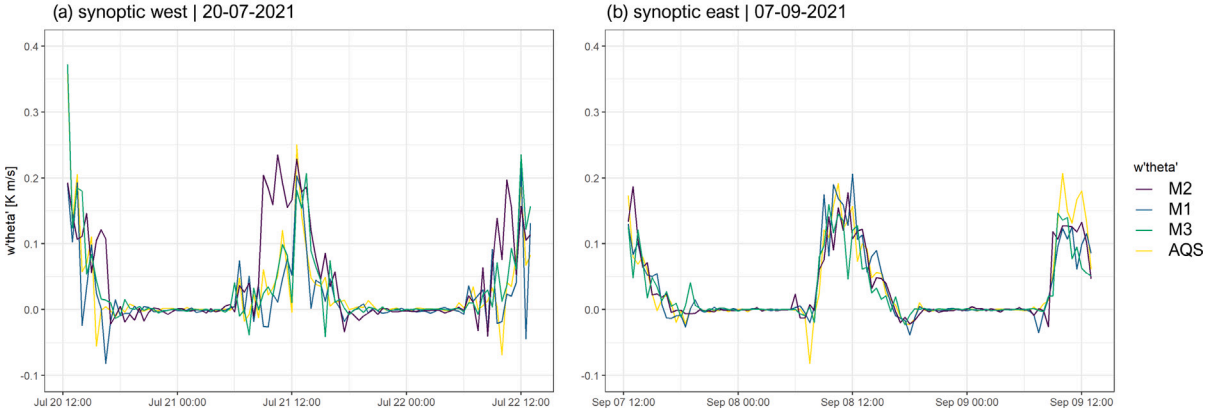

Fig. 17. Simulated time series of turbulent sensible heat flux along the street canyon at measurement locations from north to south. (a) synoptic west forcing (20 July 2021) and (b) synoptic east forcing (7 September 2021). The color scale indicates the magnitude of Q_H within the canyon cross section.

3.4.7. Dispersion of NO_2

The NO_2 concentrations associated with this airflow regime are significantly lower than those observed under westerly synoptic forcing conditions. Under local northwesterly flow, concentrations rise only to 40.0 μg m^{-3} during the morning traffic peak at 06:00 and to 45.0 μg m^{-3} during the evening peak at 18:00. In contrast, the local westerly airflow regime does not reach these thresholds within the street canyon and exhibits the lowest NO_2 concentrations among all regimes. During daytime periods between traffic peaks, concentrations fall below the 40 μg m^{-3} threshold. As illustrated in Fig. 13, this results in a difference of approximately a factor of 1.5 for local northwesterly flow and up to a factor of 2.0 for local westerly flow when compared to synoptic westerly conditions. We attribute these substantial differences, on the one hand, to the pronounced occurrence of TKE, partly driven by elevated sensible heat flux and vehicle-induced turbulence. On the other hand, we expect the vortex circulation within the street canyon to play a critical role by continuously mixing in fresh air, thereby contributing to lower pollutant concentrations.

Based on modeled results, it can be reasoned that atmospheric processes may influence NO_2 concentrations differently on the eastern side of the AQS within the street canyon. This difference can be attributed to the direction of the turbulent eddy simulated by the LES model (see Fig. 7), as well as to the direction of traffic flow. On the western side of the street canyon, traffic moves from the tunnel towards the AQS, while on the eastern side, it moves towards the tunnel. In this configuration, NO_2 emissions from vehicle exhausts on the eastern side may be more effectively mixed away while crossing the canyon, resulting in air parcels that are less enriched in NO_2 compared to those emerging directly from the tunnel. Consequently, the positioning of the AQS is critical in the context of potential exceedance of European threshold limits.

4. Conclusion

Urban street canyons, defined by narrow streets enclosed by tall buildings, frequently experience elevated NO_2 concentrations due to limited pollutant dispersion. This study highlights the complex interactions between urban morphology, traffic emissions, and atmospheric transport processes that critically shape air quality within these environments. Our findings emphasize that understanding the dynamics of airflow and turbulence is essential for developing effective strategies to mitigate NO_2 pollution in urban areas. Our combination of methods may be used at other locations to arrive at generalized results. We investigated the mechanisms contributing to the long-term exceedance of annual mean NO_2 threshold values and found that atmospheric processes play a dominant role. Notably, our results demonstrate a direct and consistent relationship between NO_2 concentrations and local flow and turbulence regimes. As no significant connection to large-scale synoptic conditions was identified, we conclude that the airflow within the street canyon operates decoupled of broader meteorological patterns. Street canyon flow is independent from synoptic flow direction and speed when large-scale forcing is weak. Accordingly, the research question posed in Section 1 can be answered as follows: Our analysis shows that a northerly airflow occurs 44% of the time during the study period within the investigated street canyon. This dominant local flow emerges even when synoptic forcing originates from the west or other directions, ultimately turning into the prevailing northerly flow. It is characterized by weak wind speeds and the formation of cross-canyon vortices that inhibit vertical mixing and trap pollutants near the surface. Such airflow conditions are associated with elevated NO_2 concentrations, with mean daily values reaching up to 72 μg^{-3} (see Fig. 13).

A novel approach to evaluate causal links between traffic activity and turbulence generation has proven impact of vehicle-induced turbulence on diurnal NO_2 variations. NO_2 concentrations are consistently lower in the early morning compared to the afternoon across all airflow regimes. This phenomenon can be attributed to the higher vehicle-induced turbulence kinetic energy as a result of higher vehicle speeds during the morning hours, which enhances pollutant dispersion. In contrast, lower vehicle speeds in the afternoon reduce TKE, leading to diminished turbulent mixing and subsequent accumulation of NO_2.

While atmospheric transport governs the overall NO_2 concentration, vehicle movement and traffic patterns play a significant role in shaping the diurnal variation of NO_2 levels within the street canyon. These insights highlight the critical importance of integrating urban design with traffic management to effectively reduce NO_2 pollution in street canyons. The proposed metric of vehicle-seconds, which provides a robust, non-linear predictor of effective NO_2 concentrations regardless of weekday, inflow, or seasonal variation, underscores the value of data-driven mitigation strategies. Reducing overall traffic volume, modernizing the vehicle fleet towards low-emission technologies, and increasing average driving speeds to shorten vehicle residence time in congested areas emerge as effective measures to lower emissions. Additionally, enhancing turbulent mixing – potentially through targeted modifications to the existing urban structure to allow greater cross-canyon airflow – could improve pollutant dispersion. These findings are particularly timely in light of the revised Ambient Air Quality Directive (as of April 9, 2024), which will enforce a more stringent annual limit of 20 μg^{-3} for NO_2 by 2030 (Deutsche Umwelthilfe, 2024). This regulatory tightening reinforces the need for integrated modeling approaches and evidence-based urban planning to ensure compliance with future air quality standards and to safeguard public health in densely built environments. Since the problem of excessive NO_2 pollution in the study area in Munich arises from a combination of extremely high traffic-related emissions and severely restricted atmospheric transport and mixing, targeted mitigation strategies must address both emission reduction and improved ventilation within the street canyon.

Funding

This study was conducted within the framework of the REINELUFFT? project (reference number TLK01-L-76330, subproject AIR) funded by the Bavarian State Ministry of the Environment and Consumer Protection. The authors gratefully acknowledge the Gauss Centre for Supercomputing e.V. (https://www.gauss-centre.eu) for supporting this project by providing computing time on the GCS Supercomputer SuperMUC-NG at Leibniz Supercomputing Centre (https://www.lrz.de).

CRediT authorship contribution statement

Leyla Sungur: Writing – original draft, Visualization, Validation, Software, Methodology, Investigation, Formal analysis, Conceptualization. **Ines Bamberger:** Software, Investigation, Data curation. **Johann Schneider:** Investigation, Data curation. **Frederik Bachmann:** Data curation. **Anke C. Nölscher:** Writing – review & editing, Validation, Data curation. **Christoph K. Thomas:** Writing – review & editing, Visualization, Supervision, Software, Resources, Investigation, Funding acquisition, Formal analysis, Data curation, Conceptualization.

Declaration of competing interest

The authors declare that they have no known competing financial interests or personal relationships that could have appeared to influence the work reported in this paper.

Acknowledgments

The authors would like to thank Gilbert Brietzke for cooperation in geodata preparation specifically designed for PALM-4U. The authors gratefully acknowledge the support from the PALM group of Leibniz University Hannover and the technical support from the Leibniz Supercomputing Centre (www.lrz.de).

References

Amato, F., Schaap, M., Reche, C., Querol, X., 2013. Road traffic: A major source of particulate matter in Europe. In: Urban Air Quality in Europe. Springer Berlin Heidelberg, Berlin, Heidelberg, ISBN: 978-3-642-38451-6, pp. 165–193. http://dx.doi.org/10.1007/698_2012_211.

Amritha, S., Varikoden, H., Patel, V., Kuttippurath, J., Gopikrishnan, G., 2024. Global, regional and city scale changes in atmospheric NO_2 with environmental laws and policies. Sustain. Cities Soc. (ISSN: 2210-6707) 112, 105617. http://dx.doi.org/10.1016/j.scs.2024.105617, URL https://www.sciencedirect.com/science/article/pii/S2210670724004426.

Anenberg, S.C., Mohegh, A., Goldberg, D.L., Kerr, G.H., Brauer, M., Burkart, K., Hystad, P., Larkin, A., Wozniak, S., Lamsal, L., 2022. Long-term trends in urban NO2 concentrations and associated paediatric asthma incidence: estimates from global datasets. Lancet Planet. Health (ISSN: 2542-5196) 6 (1), e49–e58. http://dx.doi.org/10.1016/S2542-5196(21)00255-2, URL https://www.sciencedirect.com/science/article/pii/S2542519621002552.

Anttila, P., Tuovinen, J.-P., Niemi, J.V., 2011. Primary NO2 emissions and their role in the development of NO2 concentrations in a traffic environment. Atmos. Environ. (ISSN: 1352-2310) 45 (4), 986–992. http://dx.doi.org/10.1016/j.atmosenv.2010.10.050, URL https://www.sciencedirect.com/science/article/pii/S1352231010009362.

Baldasano, J.M., Gonçalves, M., Soret, A., Jiménez-Guerrero, P., 2010. Air pollution impacts of speed limitation measures in large cities: The need for improving traffic data in a metropolitan area. Atmos. Environ. (ISSN: 1352-2310) 44 (25), 2997–3006. http://dx.doi.org/10.1016/j.atmosenv.2010.05.013, URL https://www.sciencedirect.com/science/article/pii/S1352231010003869.

Bayerisches Staatsministerium für Umwelt und Verbraucherschutz, 2025. Aktuelle Messwerte und Daten zur Luftqualität (Immissionen). Luftüberwachungssystem Bayern (LÜB). URL https://www.lfu.bayern.de/luft/immissionsmessungen/messwerte/index.htm.

Bazdidi-Tehrani, F., Masoumi-Verki, S., Gholamalipour, P., 2020. Impact of opening shape on airflow and pollutant dispersion in a wind-driven cross-ventilated model building: Large eddy simulation. Sustain. Cities Soc. (ISSN: 2210-6707) 61, 102196. http://dx.doi.org/10.1016/j.scs.2020.102196, URL https://www.sciencedirect.com/science/article/pii/S2210670720301839.

Casquero-Vera, J., Lyamani, H., Titos, G., Borrás, E., Olmo, F., Alados-Arboledas, L., 2019. Impact of primary NO2 emissions at different urban sites exceeding the European NO2 standard limit. Sci. Total Environ. (ISSN: 0048-9697) 646, 1117–1125. http://dx.doi.org/10.1016/j.scitotenv.2018.07.360, URL https://www.sciencedirect.com/science/article/pii/S0048969718328560.

Chung, T.N.H., Liu, C.-H., 2013. On the mechanism of air pollutant removal in two-dimensional idealized street canyons: A large-eddy simulation approach. Bound.-Layer Meteorol. (ISSN: 0006-8314) 148 (1), 241–253. http://dx.doi.org/10.1007/s10546-013-9811-4.

Costa, L.G., Cole, T.B., Dao, K., Chang, Y.-C., Coburn, J., Garrick, J.M., 2020. Effects of air pollution on the nervous system and its possible role in neurodevelopmental and neurodegenerative disorders. Pharmacol. Ther. (ISSN: 0163-7258) 210, 107523. http://dx.doi.org/10.1016/j.pharmthera.2020.107523, URL https://www.sciencedirect.com/science/article/pii/S0163725820300516.

Costa, S., Ferreira, J., Silveira, C., Costa, C., Lopes, D., Relvas, H., Borrego, C., Roebeling, P., Miranda, A.I., Teixeira, J.P., 2014. Integrating health on air quality assessment—Review report on health risks of two major European outdoor air pollutants: PM and NO2. J. Toxicol. Environ. Health, Part B 17 (6), 307–340. http://dx.doi.org/10.1080/10937404.2014.946164, PMID: 25333993.

Dai, Y., Cai, X., Zhong, J., Mazzeo, A., MacKenzie, A.R., 2022. Chemistry, transport, emission, and shading effects on NO2 and Ox distributions within urban canyons. Environ. Pollut. (ISSN: 0269-7491) 315, 120347. http://dx.doi.org/10.1016/j.envpol.2022.120347, URL https://www.sciencedirect.com/science/article/pii/S0269749122015615.

Deutsche Umwelthilfe, 2024. Stricter EU air quality limits by 2030: What cities must prepare for. https://www.duh.de. (Accessed 15 May 2025).

Di, Q., Wang, Y., Zanobetti, A., Wang, Y., Koutrakis, P., Choirat, C., Dominici, F., Schwartz, J.D., 2017. Air pollution and mortality in the medicare population. N. Engl. J. Med. 376 (26), 2513–2522. http://dx.doi.org/10.1056/NEJMoa1702747, URL https://www.nejm.org/doi/full/10.1056/NEJMoa1702747.

El-Hansali, Y., Farrag, S., Yasar, A., Malik, H., Shakshuki, E., Al-Abri, K., 2021. Assessment of the traffic enforcement strategies impact on emission reduction and air quality. Procedia Comput. Sci. (ISSN: 1877-0509) 184, 549–556. http://dx.doi.org/10.1016/j.procs.2021.03.068, URL https://www.sciencedirect.com/science/article/pii/S1877050921007006. The 12th International Conference on Ambient Systems, Networks and Technologies (ANT) / The 4th International Conference on Emerging Data and Industry 4.0 (EDI40) / Affiliated Workshops.

Fino, A., 2019. Air quality legislation. In: Nriagu, J. (Ed.), Encyclopedia of Environmental Health (Second Edition), second ed. Elsevier, Oxford, ISBN: 978-0-444-63952-3, pp. 61–70. http://dx.doi.org/10.1016/B978-0-12-409548-9.11045-0, URL https://www.sciencedirect.com/science/article/pii/B9780124095489110450.

Foken, T., 2021. Micrometeorology, second ed. In: Springer Atmospheric Sciences, Springer, http://dx.doi.org/10.1007/978-3-030-51989-4.

Font, A., Fuller, G.W., 2016. Did policies to abate atmospheric emissions from traffic have a positive effect in London? Environ. Pollut. (ISSN: 0269-7491) 218, 463–474. http://dx.doi.org/10.1016/j.envpol.2016.07.026, URL https://www.sciencedirect.com/science/article/pii/S0269749116305966.

Graf, M., Kossmann, M., Trusilova, K., Mühlbacher, G., 2016. Identification and climatology of alpine pumping from a regional climate simulation. Front. Earth Sci. (ISSN: 2296-6463) 4-2016, http://dx.doi.org/10.3389/feart.2016.00005, URL https://www.frontiersin.org/journals/earth-science/articles/10.3389/feart.2016.00005.

Grylls, T., Le Cornec, C.M., Salizzoni, P., Soulhac, L., Stettler, M.E., van Reeuwijk, M., 2019. Evaluation of an operational air quality model using large-eddy simulation. Atmos. Environ.: X (ISSN: 2590-1621) 3, 100041. http://dx.doi.org/10.1016/j.aeaoa.2019.100041, URL https://www.sciencedirect.com/science/article/pii/S2590162119300449.

Guerreiro, C.B., Foltescu, V., de Leeuw, F., 2014. Air quality status and trends in Europe. Atmos. Environ. (ISSN: 1352-2310) 98, 376–384. http://dx.doi.org/10.1016/j.atmosenv.2014.09.017, URL https://www.sciencedirect.com/science/article/pii/S1352231014007109.

Huang, S., Li, H., Wang, M., Qian, Y., Steenland, K., Caudle, W.M., Liu, Y., Sarnat, J., Papatheodorou, S., Shi, L., 2021. Long-term exposure to nitrogen dioxide and mortality: A systematic review and meta-analysis. Sci. Total Environ. (ISSN: 0048-9697) 776, 145968. http://dx.doi.org/10.1016/j.scitotenv.2021.145968, URL https://www.sciencedirect.com/science/article/pii/S0048969721010354.

Hunter, L., Johnson, G., Watson, I., 1992. An investigation of three-dimensional characteristics of flow regimes within the urban canyon. Atmos. Environ. Part B. Urban Atmos. (ISSN: 0957-1272) 26 (4), 425–432. http://dx.doi.org/10.1016/0957-1272(92)90049-X, URL https://www.sciencedirect.com/science/article/pii/095712729290049X.

INFRAS, 2019. Handbook Emission Factors for Road Transport (HBEFA), Version 4.1. INFRAS, Bern, Switzerland, https://www.hbefa.net.

Kellneróva, R., Fuka, V., Uruba, V., Jurčáková, K., Nosek, Š., Chaloupecká, H., Jaňour, Z., 2018. On street-canyon flow dynamics: Advanced validation of LES by time-resolved PIV. Atmosphere (ISSN: 2073-4433) 9 (5), http://dx.doi.org/10.3390/atmos9050161, URL https://www.mdpi.com/2073-4433/9/5/161.

Kuhlmann, G., Chan, K.L., Donner, S., Zhu, Y., Schwaerzel, M., Dörner, S., Chen, J., Hueni, A., Nguyen, D.H., Damm, A., Schütt, A., Dietrich, F., Brunner, D., Liu, C., Buchmann, B., Wagner, T., Wenig, M., 2022. Mapping the spatial distribution of NO_2 with in situ and remote sensing instruments during the munich NO_2 imaging campaign. Atmos. Meas. Tech. 15 (6), 1609–1629. http://dx.doi.org/10.5194/amt-15-1609-2022, URL https://amt.copernicus.org/articles/15/1609/2022/.

Kurtenbach, R., Kleffmann, J., Niedojadlo, A., Wiesen, P., 2012. Primary NO2 emissions and their impact on air quality in traffic environments in Germany. Environ. Sci. Eur. (ISSN: 2190-4715) 24 (1), 21. http://dx.doi.org/10.1186/2190-4715-24-21.

Liu, W., Shi, N., Wang, H., Huang, Q., 2024. Thermodynamic characteristics of extreme heat waves over the middle and lower reaches of the Yangtze River Basin. Clim. Dyn. (ISSN: 0930-7575) 62, 3877–3889. http://dx.doi.org/10.1007/s00382-024-07104-6.

Maronga, B., Banzhaf, S., Burmeister, C., Esch, T., Forkel, R., Fröhlich, D., Fuka, V., Gehrke, K.F., Geletič, J., Giersch, S., Gronemeier, T., Groß, G., Heldens, W., Hellsten, A., Hoffmann, F., Inagaki, A., Kadasch, E., Kanani-Sühring, F., Ketelsen, K., Khan, B.A., Knigge, C., Knoop, H., Krč, P., Kurppa, M., Maamari, H., Matzarakis, A., Mauder, M., Pallasch, M., Pavlik, D., Pfafferott, J., Resler, J., Rissmann, S., Russo, E., Salim, M., Schrempf, M., Schwenkel, J., Seckmeyer, G., Schubert, S., Sühring, M., von Tils, R., Vollmer, L., Ward, S., Witha, B., Wurps, H., Zeidler, J., Raasch, S., 2020. Overview of the PALM model system 6.0. Geosci. Model. Dev. 13 (3), 1335–1372. http://dx.doi.org/10.5194/gmd-13-1335-2020, URL https://gmd.copernicus.org/articles/13/1335/2020/.

Maronga, B., Gross, G., Raasch, S., Banzhaf, S., Forkel, R., Heldens, W., Kanani-Suehring, F., Matzarakis, A., Mauder, M., Pavlik, D., Pfafferott, J., Schubert, S., Seckmeyer, G., Sieker, H., Winderlich, K., 2019. Development of a new urban climate model based on the model PALM - Project overview, planned work, and first achievements. Meteorol. Z. 28 (2), 105–119. http://dx.doi.org/10.1127/metz/2019/0909.

Maronga, B., Gryschka, M., Heinze, R., Hoffmann, F., Kanani-Sühring, F., Keck, M., Ketelsen, K., Letzel, M.O., Sühring, M., Raasch, S., 2015. The Parallelized Large-Eddy Simulation Model (PALM) version 4.0 for atmospheric and oceanic flows: model formulation, recent developments, and future perspectives. Geosci. Model. Dev. 8 (8), 2515–2551. http://dx.doi.org/10.5194/gmd-8-2515-2015, URL https://gmd.copernicus.org/articles/8/2515/2015/.

Martínez-Sánchez, Á., Lazpita, E., Corrochano, A., Le Clainche, S., Hoyas, S., Vinuesa, R., 2023. Data-driven assessment of arch vortices in simplified urban flows. Int. J. Heat Fluid Flow (ISSN: 0142-727X) 100, 109101. http://dx.doi.org/10.1016/j.ijheatfluidflow.2022.109101, URL https://www.sciencedirect.com/science/article/pii/S0142727X22001692.

METEK GmbH, 2023. uSonic-3 Class A: 3D ultrasonic anemometer. URL https://metek.de/de/product/usonic-3-class-a/. (Accessed May 13 2025).

METER Group, Inc., 2021. ClimaVUE™ 50 Weather Sensor. https://www.metergroup.com/environment/products/climavue-50/. (Accessed May 13 2025).

Moonen, P., Gromke, C., Dorer, V., 2013. Performance assessment of Large Eddy Simulation (LES) for modeling dispersion in an urban street canyon with tree planting. Atmos. Environ. (ISSN: 1352-2310) 75, 66–76. http://dx.doi.org/10.1016/

j.atmosenv.2013.04.016, URL https://www.sciencedirect.com/science/article/pii/S1352231013002616.

Okaze, T., Kikumoto, H., Ono, H., Imano, M., Ikegaya, N., Hasama, T., Nakao, K., Kishida, T., Tabata, Y., Nakajima, K., Yoshie, R., Tominaga, Y., 2021. Large-eddy simulation of flow around an isolated building: A step-by-step analysis of influencing factors on turbulent statistics. Build. Environ. (ISSN: 0360-1323) 202, 108021. http://dx.doi.org/10.1016/j.buildenv.2021.108021, URL https://www.sciencedirect.com/science/article/pii/S0360132321004248.

Oke, T.R., Mills, G., Christen, A., Voogt, J.A., 2017. Urban Climates. Cambridge University Press.

Pandey, S.K., Singh, J., 2021. Chapter 22 - Nitrogen dioxide: Risk assessment, environmental, and health hazard. In: Singh, J., Kaushik, R., Chawla, M. (Eds.), Hazardous Gases. Academic Press, ISBN: 978-0-323-89857-7, pp. 273–288. http://dx.doi.org/10.1016/B978-0-323-89857-7.00001-3, URL https://www.sciencedirect.com/science/article/pii/B9780323898577000013.

Phoenix, G.K., Emmett, B.A., Britton, A.J., Caporn, S.J.M., Dise, N.B., Helliwell, R., Jones, L., Leake, J.R., Leith, I.D., Sheppard, L.J., Sowerby, A., Pilkington, M.G., Rowe, E.C., Ashmore, M.R., Power, S.A., 2012. Impacts of atmospheric nitrogen deposition: responses of multiple plant and soil parameters across contrasting ecosystems in long-term field experiments. Global Change Biol. 18 (4), 1197–1215. http://dx.doi.org/10.1111/j.1365-2486.2011.02590.x, arXiv:https://onlinelibrary.wiley.com/doi/pdf/10.1111/j.1365-2486.2011.02590.x.

Pültz, J., Thürkow, M., Banzhaf, S., Schaap, M., 2025. Nitrogen dioxide source attribution for urban and regional background locations across Germany. Atmosphere (ISSN: 2073-4433) 16 (3), http://dx.doi.org/10.3390/atmos16030312, URL https://www.mdpi.com/2073-4433/16/3/312.

Steinfeld, D., Boettcher, M., Forbes, R., Pfahl, S., 2020. The sensitivity of atmospheric blocking to upstream latent heating – numerical experiments. Weather. Clim. Dyn. 1 (2), 405–426. http://dx.doi.org/10.5194/wcd-1-405-2020, URL https://wcd.copernicus.org/articles/1/405/2020/.

Stewart, G.B., Dajnak, D., Davison, J., Carslaw, D.C., Beddows, A.V., Phantawesak, N., Stettler, M.E., Hollaway, M.J., Beevers, S.D., 2024. New NOx and NO2 vehicle emission curves, and their implications for emissions inventories and air pollution modelling. Urban Clim. (ISSN: 2212-0955) 57, 102103. http://dx.doi.org/10.1016/j.uclim.2024.102103, URL https://www.sciencedirect.com/science/article/pii/S2212095524003006.

Sun, W., Lu, K., Li, R., 2024. Global estimates of ambient NO2 concentrations and long-term health effects during 2000–2019. Environ. Pollut. (ISSN: 0269-7491) 359, 124562. http://dx.doi.org/10.1016/j.envpol.2024.124562, URL https://www.sciencedirect.com/science/article/pii/S0269749124012764.

Sungur, L., Babel, W., Späte, E., Schneider, J., Thomas, C.K., 2025. Climate sensitive designs for policy makers: How LES model resolution affects accuracy in capturing urban micro-scale weather during heatwaves. Urban Clim. (ISSN: 2212-0955) 61, 102400. http://dx.doi.org/10.1016/j.uclim.2025.102400, URL https://www.sciencedirect.com/science/article/pii/S2212095525001166.

Transportation Research Board, 2010. Highway Capacity Manual, 2010 ed. National Academies of Sciences, Engineering, Washington D.C., ISBN: 0309160774, URL http://hcm.trb.org/?qr=1.

Vermessungsverwaltung, B., 2024. ALKIS - Tatsaechliche Nutzung (TN). URL https://geoservices.bayern.de/od/wms/alkis/v1/tn?.

von Nieding, G., Wagner, M., Krekeler, H., Smidt, U., Muysers, K., 1970. Grenzwertbestimmung der akuten NO2-Wirkung auf den respiratorischen Gasaustausch und die Atemwegswiderstände des chronisch lungenkranken Menschen. In: Internationales Archiv für Arbeitsmedizin / International Archives of Occupational Health. Springer Berlin Heidelberg, Berlin, Heidelberg, ISBN: 978-3-662-38021-5, pp. 700–710. http://dx.doi.org/10.1007/978-3-662-38021-5_51.

Wang, Y., Wang, T., Gu, Q., Shang, J., 2025. Adsorption removal of NO2 under low-temperature and low-concentration conditions: A review of adsorbents and adsorption mechanisms. Adv. Mater. 37 (5), 2401623. http://dx.doi.org/10.1002/adma.202401623, arXiv:https://advanced.onlinelibrary.wiley.com/doi/pdf/10.1002/adma.202401623.

Xie, X., Huang, Z., 2007. Impact of aspect ratio and surface heating on pollutant transport in street canyons. J. Mech. Sci. Technol. (ISSN: 1738-494X) 21 (11), 1781–1790. http://dx.doi.org/10.1007/BF03177433, 18th International Symposium on Transport Phenomena (ISTP 18), Daejon, South Korea, Aug 27–30, 2007.

Yang, B., Zhang, K.M., Xu, W.D., Zhang, S., Batterman, S., Baldauf, R.W., Deshmukh, P., Snow, R., Wu, Y., Zhang, Q., Li, Z., Wu, X., 2018. On-road chemical transformation as an important mechanism of NO2 formation. Environ. Sci. Technol. (ISSN: 1520-5851) 52 (8), 4574–4582. http://dx.doi.org/10.1021/acs.est.7b05648.

Zhang, Z., Li, Q., Hu, Q., Xue, J., Liu, T., Tang, Z., Wang, F., Zhang, C., Lu, C., Wang, Z., Gao, M., Liu, C., 2025. Deep learning approach for reconstructing three-dimensional distribution of NO2 on an urban scale. Remote Sens. Environ. (ISSN: 0034-4257) 321, 114678. http://dx.doi.org/10.1016/j.rse.2025.114678, URL https://www.sciencedirect.com/science/article/pii/S0034425725000823.

Zhiyin, Y., 2015. Large-eddy simulation: Past, present and the future. Chin. J. Aeronaut. (ISSN: 1000-9361) 28 (1), 11–24. http://dx.doi.org/10.1016/j.cja.2014.12.007, URL https://www.sciencedirect.com/science/article/pii/S1000936114002064.